

Topological Control of Quantum Chaos Diagnostics: OTOCs, Spectral Statistics, and Information Scrambling in Ising Model

Reza Pirmoradian,^{a,b} Soheir Rouhani,^{c,d} M. Reza Tanhayi^{a,e,f}

^a*School of Quantum Physics and Matter Institute for Research in Fundamental Sciences (IPM), P.O. Box 19395-5531, Tehran, Iran*

^b*Ershad Damavand, Institute of Higher Education (EDI) P.O. Box 14168-34311, Tehran, Iran*

^c*Department of Mathematics and Computer Science, Amirkabir University of Technology, Tehran, Iran*

^d*Department of Mathematics, Faculty of Mathematical Sciences, Alzahra University, Tehran, Iran*

^e*Department of Physics, CT.C, Islamic Azad University, Tehran, Iran P.O. Box 14676-86831, Tehran, Iran*

^f*Institute of Biosocial and Quantum Science and Technologies, CT.C, Islamic Azad University, Tehran, Iran*

E-mail: rezapirmoradian@ipm.ir, So.rouhani@aut.ac.ir, mtanhayi@ipm.ir

ABSTRACT: We investigate the integrability-to-chaos transition and information scrambling in Ising spin networks via a graph-theoretic formulation. Modeling spins as vertices and interactions via adjacency matrices across path, Erdős–Rényi, and Watts–Strogatz topologies, we demonstrate that long-range couplings and heterogeneous degree distributions drastically accelerate quantum information propagation. The Hamiltonian comprises local and normalized non-local interactions; tuning the non-local coupling and field heterogeneity drives integrability breaking. To quantify scrambling, we employ bipartite mutual and tripartite information. Increasing non-local interactions drives tripartite information to large negative values, signaling deep information scrambling. Out-of-time-order correlators (OTOCs) exhibit exponential early-time growth, yielding quantum Lyapunov exponents that scale systematically with parameters governing the chaotic regime. Complementing this, Krylov complexity reveals rapid operator growth in the chaotic phase, synchronizing with OTOC and mutual information dynamics. Spectrally, the transition manifests as a shift from Poissonian to Wigner–Dyson level spacing statistics. The spectral form factor (SFF) exhibits the characteristic slope-dip-ramp-plateau structure, enabling the extraction of Thouless and Heisenberg times. Crucially, a reduced Thouless time strongly correlates with accelerated informational and operator scrambling. Ultimately, this work establishes a unified framework bridging network topology with information-theoretic, operator, and spectral diagnostics, offering profound insights into thermalization and non-equilibrium dynamics in quantum many-body systems.

Contents

1	Introduction	1
2	The Ising Model and the Analysis of Integrability and Chaos	5
3	Entanglement Dynamics and Entropy Growth	8
4	OTOC and chaos diagnostics	12
5	Krylov complexity, spectral diagnostics of chaos, and their connection to entanglement	15
6	Spectral diagnostics of chaos, the SFF, and their connection to entanglement growth and operator complexity	19
7	Conclusion	25

1 Introduction

Research on isolated Non-Equilibrium Quantum Systems has, over the past two decades, established itself as a central frontier in both theoretical and experimental physics. These systems provide a fundamental framework for analyzing information scrambling, entanglement growth, quantum energy diffusion, and chaotic behavior under far-from-equilibrium conditions [1–5]. Unlike classical systems, whose evolution is governed by nonlinear differential equations and chaos theory, the dynamics of closed quantum systems are constrained by the unitary, reversible Schrödinger equation:

$$i\hbar \frac{\partial}{\partial t} |\psi(t)\rangle = \hat{H} |\psi(t)\rangle. \quad (1.1)$$

where $|\psi(t)\rangle$ represents the time-dependent state vector and \hat{H} denotes the system Hamiltonian.

The inherent reversibility of unitary dynamics poses a fundamental paradox: how do irreversible thermodynamic behaviors, including subsystem thermalization and signatures of quantum chaos, emerge from underlying reversible quantum evolution? Tracing back from Boltzmann’s foundational work on classical ergodicity to modern frameworks, this issue remains a cornerstone of theoretical physics. In the context of isolated quantum many-body systems, the Eigenstate Thermalization Hypothesis (ETH) has emerged as the prevailing explanation, suggesting that thermal properties are encoded within individual eigenstates, thereby reconciling microscopic reversibility with macroscopic irreversibility [6, 7].

A paradigmatic protocol for investigating these non-equilibrium dynamics and testing the validity of thermalization hypotheses is the Quantum Quench. In this setup, the system is initialized in a well-defined state, typically the ground state of a pre-quench Hamiltonian, before a control parameter—such as the external field strength or spin–spin interaction—is abruptly varied. Following the quench, the state evolves unitarily under the post-quench Hamiltonian \hat{H}' , driving the system far from equilibrium. The central objective is to analyze the long-time relaxation of local observables and entanglement entropy to determine whether the system thermalizes to a state describable by standard statistical ensembles. This framework has become indispensable not only for theoretical advancements but also for experimental realizations in quantum simulators based on trapped ions, ultracold atoms, and photonic systems. [8–12].

Despite the significance of this approach, the present study is focused on alternative methods that employ Ising models and tools from graph theory. Prototypical interacting Hamiltonians, such as the Ising model, serve as a controlled platform for investigating collective behavior, correlation dynamics, and the validity of thermalization hypotheses. Concurrently, a graph-theoretical framework provides structural and topological instruments to quantify network properties and the complexity of the underlying interaction landscape. This synergy enables a precise examination of the transition between integrable and chaotic regimes, specifically elucidating how structural connectivity influences the onset of quantum chaos and eigenstate thermalization. Consequently, the integration of these approaches offers a rigorous pathway to deciphering the mechanistic origins of thermalization and distinguishing the fundamental characteristics of integrable versus non-integrable systems.

The nature of the Hamiltonian has a crucial impact on the system’s dynamics. If the Hamiltonian is integrable, an infinite set of independent conserved quantities I_j prevents the system from undergoing complete thermalization. In this case, the asymptotic state is described by Generalized Gibbs Ensemble (GGE):

$$\rho_{GGE} = \frac{1}{\mathcal{Z}} \exp\left(-\sum_j \lambda_j I_j\right) \quad (1.2)$$

where λ_j are Lagrange multipliers fixed by the initial expectation values of the conserved charges [13–16]. By contrast, non-integrable (chaotic) systems lack these additional constraints and typically thermalize to an equilibrium described by the conventional Gibbs ensemble:

$$\rho = \frac{1}{\mathcal{Z}} e^{-\beta \hat{H}} \quad (1.3)$$

This dichotomy underpins the ETH. The ETH posits that in chaotic systems, the matrix elements of local observables in the energy eigenbasis vary smoothly with energy, with off-diagonal fluctuations exponentially suppressed by the entropy, thereby ensuring that individual eigenstates encode thermal properties [17, 18].

A paradigmatic system facilitating the investigation of these phenomena is the one-dimensional Ising chain subject to both transverse and longitudinal magnetic fields. The

system is governed by the Hamiltonian:

$$\hat{H} = -J \sum_{i=1}^{N-1} \hat{\sigma}_i^z \hat{\sigma}_{i+1}^z - h_x \sum_{i=1}^N \hat{\sigma}_i^x - h_z \sum_{i=1}^N \hat{\sigma}_i^z \quad (1.4)$$

where J denotes the spin–spin coupling strength, h_x the transverse field, and h_z the longitudinal field. In the absence of the longitudinal field ($h_z = 0$), the model is integrable and can be exactly solved by mapping onto free fermions via the Jordan–Wigner transformation. Conversely, introducing a non-zero longitudinal field ($h_z \neq 0$) breaks integrability by destroying the extensive set of conservation laws. This drives the system into a non-integrable regime characterized by quantum chaos and thermalizing dynamics, thereby providing a controlled testbed for examining the validity of the ETH [19–22].

Quantum entanglement entropy serves as a fundamental diagnostic for probing non-equilibrium dynamics and thermalization in isolated quantum systems. For a subsystem A with reduced density matrix ρ_A

$$\rho_A(t) = \text{Tr}_B |\psi(t)\rangle \langle \psi(t)| \quad (1.5)$$

The von Neumann entropy is defined as follows:

$$\mathcal{S}_A(t) = -\text{Tr}(\rho_A(t) \ln \rho_A(t)) \quad (1.6)$$

Similarly, the Rényi entropy of order α is defined as:

$$\mathcal{S}_\alpha(\rho_A) = \frac{1}{1-\alpha} \ln(\text{Tr} \rho_A^\alpha) \quad (1.7)$$

In integrable systems, the von Neumann entropy of subsystems typically exhibits linear growth at early times, where the growth rate is bounded by the quasiparticle propagation velocity as dictated by the Lieb–Robinson bound [23–25]. In contrast, chaotic non-integrable systems display rapid information scrambling. The entropy grows linearly before saturating at late times to a value approaching the Page value, which describes the average entropy of random states and signifies thermalization consistent with the ETH [26–28].

In addition to single-body measures, mutual information between subsystems serves as a rigorous probe for tracking the spread and dispersion of quantum information. The bipartite mutual information between two subsystems quantifies the amount of information shared between them, and its temporal behavior reflects how correlations are established and disentangled. In systems where quasiparticles propagate and information transfer occurs along a light cone structure, the bipartite mutual information between distant regions increases with a delayed, approximately linear-in-time pattern, sometimes accompanied by revivals or oscillations—a feature that is particularly pronounced in integrable systems. In chaotic systems adhering to the ETH, the bipartite mutual information is typically distributed more broadly and more rapidly, and it converges to smaller values on short timescales, indicating the rapid “scrambling” of information throughout the entire system.

The tripartite information serves as a more sensitive diagnostic that quantifies the delocalization of information shared among three subsystems and the manner in which that

information is distributed. The magnitude of this quantity—and in particular its sign—is employed as a key indicator of information scrambling: in chaotic systems where information is rapidly scrambled and broadly dispersed across all degrees of freedom, the tripartite information typically becomes negative. This negativity signals the monogamy of mutual information, indicative of information delocalization and the extensive fragmentation of its distribution characteristic of thermalizing dynamics. By contrast, in integrable regimes, this quantity remains smaller in magnitude (i.e., less negative) or even non-negative, consistent with the presence of stable quasiparticle structures, local conservation laws, and information revivals. Consequently, the temporal behavior of bipartite and tripartite information plays a complementary role, alongside entanglement entropy and other diagnostics, in distinguishing chaotic thermalizing dynamics from integrable behavior, thereby providing a comprehensive probe of the validity of the ETH framework.

To characterize quantum chaos and information scrambling, complementary diagnostic tools have been established. A primary measure is the OTOC:

$$C(t) = -\langle [\hat{W}(t), \hat{V}(0)]^2 \rangle \quad (1.8)$$

where the operator evolves as $\hat{W}(t) = e^{i\hat{H}t}\hat{W}e^{-i\hat{H}t}$. In the scrambling regime of chaotic systems, $C(t)$ typically exhibits exponential growth:

$$C(t) \sim e^{\lambda_L t} \quad (1.9)$$

where λ_L denotes the quantum Lyapunov exponent. Notably, in holographic theories, its value is bounded by $\lambda_L \leq \frac{2\pi K_B T}{\hbar}$ [29–32].

Complementarily, the SFF serves as a key probe for spectral correlations and level statistics inherent to quantum chaos:

$$SFF(\beta, t) = |Z(\beta + it)|^2 \quad (1.10)$$

where $Z(\beta) = \text{Tr}[e^{-\beta\hat{H}}]$ is the partition function [33, 34].

One of the most reliable spectral diagnostics for distinguishing chaotic and integrable quantum systems is the statistics of energy-level spacings. In chaotic systems satisfying the ETH, nearest-neighbor level spacings follow well-established correlated distributions, specifically the Wigner–Dyson distribution. This indicates level ‘repulsion’—the tendency of energy levels to avoid one another—and the existence of strong spectral correlations characteristic of quantum chaos. By contrast, in integrable systems, the level spacings typically conform to the Poisson distribution; i.e., they are comparatively uncorrelated and lack pronounced level repulsion, reflecting the presence of extensive conserved quantities. This statistical deviation is widely employed as a practical diagnostic of spectral chaos and is often used in conjunction with other spectral analyses, such as the SFF.

Another recently introduced diagnostic probing operator growth is Krylov complexity. The initial operator \hat{O} is mapped, via the Liouvillian superoperator $\hat{L}A = [\hat{H}, A]$, onto a Krylov subspace spanned by:

$$|\mathcal{O}_n\rangle = \hat{L}^n |\mathcal{O}_0\rangle \quad (1.11)$$

which is then orthogonalized via the Lanczos algorithm to form a chain of orthonormal basis states. Krylov complexity is defined as the mean index of the weighted distribution in this basis:

$$K(t) = \sum_n n |a_n(t)|^2 \quad (1.12)$$

Studies indicate that $K(t)$ exhibits exponential growth in chaotic systems, reflecting rapid operator scrambling, whereas in integrable systems it remains bounded or grows polynomially with oscillatory behaviour [35–39]. This distinction makes Krylov complexity a powerful tool for characterizing the dynamical approach to thermalization and the validity of ETH.

The combination of these diagnostics—entanglement, the OTOC, the SFF, and Krylov complexity—provides a comprehensive framework for the analysis of non-equilibrium quantum systems and thermalization, exhibiting close connections to quantum information theory, holography, and quantum gravity. In this context, minimal models such as the Ising chain, despite their apparent simplicity, have become ideal laboratories for understanding complex quantum behavior. They yield deep insights into the fundamental mechanisms of quantum dynamics as well as the development of quantum technologies. [40, 41].

2 The Ising Model and the Analysis of Integrability and Chaos

The Ising model, as one of the paradigmatic patterns in statistical physics and quantum systems theory, plays a fundamental role in the analysis and understanding of one-dimensional systems. The significance of this model arises from the fact that, despite its apparent simplicity—describing a system of two-state spins that interact only with their nearest neighbors—it is capable of representing a wide range of profound physical phenomena. In its one-dimensional quantum version, often studied in the presence of a transverse field, this framework becomes a precise mathematical setting for investigating quantum phase transitions. The analytical solution of the one-dimensional Ising model, using transformations such as the Jordan-Wigner transformation and mapping to free fermions, has enabled a detailed study of spectral properties, interaction dynamics, and long-range correlation behaviors. This characteristic has made the Ising model not only a "computational tool" but also a "conceptual laboratory" for testing fundamental ideas such as spontaneous symmetry breaking, scale invariance, and coherence structure in phase transitions.

In the analysis of one-dimensional quantum systems, the Ising model constitutes one of the fundamental and indispensable tools, as it enables the study of non-equilibrium dynamics and complex phenomena such as the growth of correlations, energy transport, and quantum chaos. To investigate the onset of thermalization and the validity of the ETH, it is crucial to move beyond the integrable limit. In its most general form, the Hamiltonian of the Ising model may include both local and nonlocal interactions, explicitly breaking integrability through the introduction of a longitudinal field and all-to-all couplings. The Hamiltonian can be written as follows:

$$\hat{H} = \hat{H}_{local} - g \frac{1}{\sqrt{N}} \sum_{i < j} \hat{\sigma}_i^z \hat{\sigma}_j^z \quad (2.1)$$

where

$$\hat{H}_{local} = -J \sum_{i=1}^{N-1} \hat{\sigma}_i^z \hat{\sigma}_{i+1}^z - h_x \sum_{i=1}^N \hat{\sigma}_i^x - h_z \sum_{i=1}^N \hat{\sigma}_i^z \quad (2.2)$$

defines the local Hamiltonian. Here, J denotes the strength of the local spin–spin coupling, h_x and h_z are the transverse and longitudinal fields, respectively, g is the coefficient of the nonlocal interaction, and N denotes the total number of spins. The inclusion of the longitudinal field h_z alongside the nonlocal interaction term breaks integrability, thereby inducing quantum chaotic behavior. The nonlocal coupling is scaled by $\frac{1}{N}$ to ensure a well-defined large- N limit. This scaling maintains a robust interaction strength that drives the level statistics from Poissonian to the Wigner-Dyson distribution—a definitive signature of quantum chaos, thermalization, and the validity of the ETH [42–44].

Graph theory provides a robust framework for representing quantum states and their interaction networks. In this representation, spins are modeled as vertices, while the edges indicate the presence of interactions between them. This configuration facilitates the visualization of complex spin networks and aids in elucidating the interplay between local and global dynamics.

Within the framework of the quantum Ising model, each node (vertex) of a graph denotes a spin-1/2 degree of freedom, where the local basis states correspond to the eigenvalues $+1$ or -1 of the Pauli operator, representing spin-up and spin-down configurations. The edges of the graph encode the coupling topology between these particles. By selecting distinct graph topologies—for instance, path graphs, wheel graphs, complete graphs, or random graphs—the interaction pattern can be engineered to directly determine the resulting Hamiltonian structure and its spectral properties. To illustrate the impact of these topological choices on the energy spectrum, the sorted eigenvalues for representative models—specifically the path, complete, cycle, and random graphs—are computed and presented in Fig.1.

From a structural standpoint, the choice of graph topology dictates the system’s spectral and dynamical characteristics. Path graphs and cycle graphs model one-dimensional geometries with open and periodic boundary conditions, respectively. The complete graph, owing to its collective symmetry and vertex homogeneity, effectively reduces to a highly symmetric solvable model; consequently, it typically does not exhibit the characteristic signatures of quantum chaos observed in nonintegrable systems. In contrast, random graphs (e.g., Erdős–Rényi graphs) or structures with topological disorder can break simple mappings, providing a setting where nonintegrability and richer, complex behavior may emerge. When nonlocal interactions and the longitudinal field are switched off $g = 0, (h_z) = 0$, the system becomes integrable and, under the Jordan–Wigner transformation, maps onto a collection of free fermions. This regime possesses an infinite set of independent conserved quantities, which prevents thermalization to a standard Gibbs ensemble. Under these conditions, the system relaxes to a GGE [4, 5]. In this integrable limit, the growth of the von Neumann entropy is constrained, and long-lived oscillatory behavior is observed over time [16–18].

When nonlocal interactions $g \neq 0$ and/or a longitudinal field $h_z \neq 0$ are introduced,

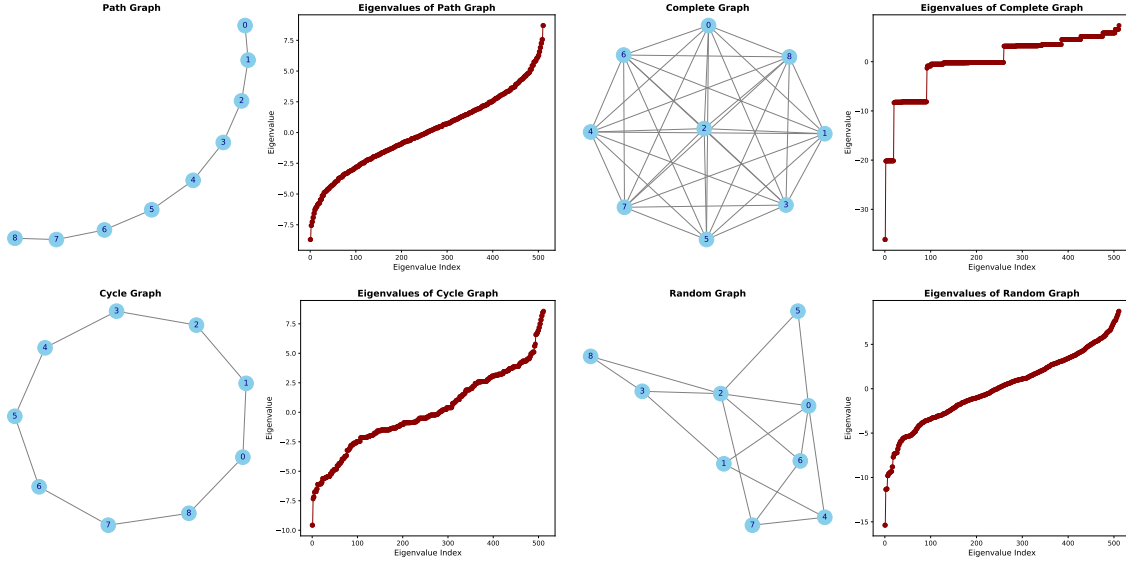


Figure 1. In this figure, the sorted eigenvalues for four graph models—the path graph, the complete graph, the Cycle graph, and a random graph—have been computed and are presented.

the integrability of the system is broken, driving it into a non-integrable, chaotic regime. In this regime, the energy spectrum develops a complex structure where spectral spacings become strongly correlated. Consequently, the level spacing distribution ceases to be Poissonian and instead follows the Wigner–Dyson distribution characteristic of the Gaussian Orthogonal Ensemble (GOE):

$$P(s) = \frac{\pi}{2} s \exp\left(-\frac{\pi}{4} s^2\right) \quad (2.3)$$

This transition is a hallmark of quantum chaos, characterized by the emergence of level repulsion and the random-matrix-like structure of the Hamiltonian [9–11]. To numerically verify this signature of quantum chaos, Fig. 2 depicts the level spacing distribution of the energy eigenvalues for four representative graph topologies (path, Erdős–Rényi, random, and Watts–Strogatz small-world networks) in the non-integrable regime. These spectral features are intimately linked to the rapid growth of entanglement entropy, a phenomenon consistently observed in both numerical simulations and experimental measurements of quantum simulators. In contrast to integrable systems, which relax to a GGE due to a macroscopic number of conserved quantities, quantum chaotic systems lack an extensive set of local integrals of motion. Consequently, the system thermalizes, and the long-time expectation values of local observables are described by the standard Gibbs ensemble, as dictated by the ETH: In contrast to integrable systems that relax to a GGE due to extensive conserved quantities, nonlocal chaotic systems lack a sufficient number of local integrals of motion. This absence causes the system to relax toward the standard thermal Gibbs ensemble, governed by the ETH.

This change in behavior is directly associated with the rapid growth of entropy, the scrambling of information, and the increase in operator complexity [12–15]. Therefore, the

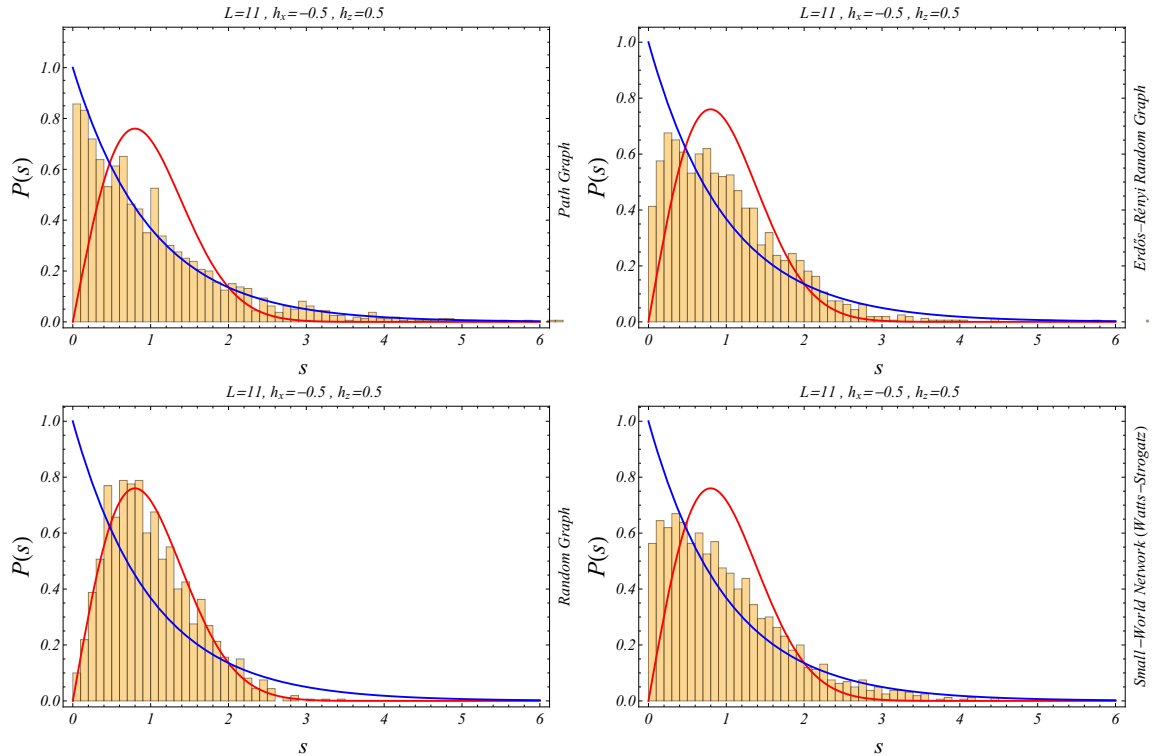


Figure 2. This figure displays the Level spacing for energy eigenvalues of the Ising models for four graph topologies: the path graph (top-left), the Erdős–Rényi graph (top-right), the random graph (bottom-left), and the Watts–Strogatz small-world network (bottom-right). The calculations and plots were performed using the parameters $h_x = -0.5$, $h_z = 0.5$, and $L = 11$.

comparative analysis of the nonlocal and local Ising models furnishes the conceptual and mathematical framework for examining diagnostics of chaos and thermalization, such as the OTOC and Krylov complexity, in subsequent sections.

The introduction of nonlocal interactions facilitates the rapid spread of correlations, driving the system toward thermal equilibrium. This behavior is manifested by pronounced changes in the growth of entropy, the rapid development of multipartite entanglement, and the exponential growth of operator size. These features underpin the validity of ETH and modern diagnostics of quantum chaos [16–18].

3 Entanglement Dynamics and Entropy Growth

A precise understanding of the dynamics of entanglement and entropy growth in nonequilibrium quantum systems plays a central role in the analysis of how quantum information spreads, how long-range correlations are established, and how operator complexity increases.

The study of these processes not only provides a means to characterize the transient behavior of far-from-equilibrium systems, but also establishes the theoretical foundation for the definition and interpretation of modern diagnostics such as OTOCs and Krylov

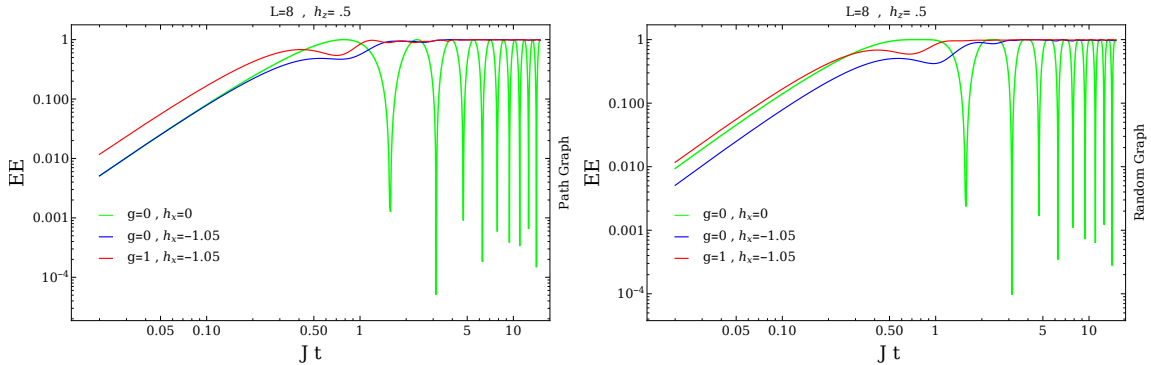


Figure 3. The entanglement-entropy dynamics of the first qubit for the Ising model defined on a path graph (left) and on a random graph (right) were computed and plotted, after averaging over 180 random initial states, using the parameters $h_z = 0.5$ and $L = 8$, as a function of the parameter Jt .

complexity. These diagnostics are regarded as subtle and efficient tools for distinguishing between integrable and chaotic dynamics, serving as quantitative measures of a system's sensitivity to local and nonlocal perturbations and its scrambling capability.

From a practical perspective, the analysis of such dynamics is closely linked to spin models, in particular to local and nonlocal Ising models and their non-integrable deformations. Within these frameworks, the time evolution of entanglement and entropy is governed not only by the microscopic features of the interactions but is also sensitive to the system's integrability and the validity of the ETH. Specifically, in integrable systems, the relaxation process is constrained by an extensive set of conserved charges, leading to a GGE rather than standard thermalization; here, the growth of entanglement entropy typically proceeds ballistically but retains memory of the initial state. In contrast, in chaotic systems satisfying ETH, the dynamics exhibit effective stochasticity described by Random Matrix Theory (RMT), accompanied by rapid information scrambling, Lyapunov-like growth of operator complexity, and saturation of entropy to thermal values consistent with the microcanonical ensemble.

Therefore, a detailed investigation of entanglement dynamics and operator complexity in nonequilibrium systems not only plays a fundamental role in elucidating the theoretical foundations of quantum chaos and modern statistical mechanics, but also establishes a unifying framework connecting quantum physics, critical field theories, and quantum information theory. This framework has, in particular, gained increasing significance in the context of one-dimensional Ising models and their generalizations, which serve as conceptual laboratories for probing the interplay between localization, thermalization, and complexity.

To this end, as shown in Fig.3, the time evolution of the entanglement entropy is presented for various Ising models. This observable serves as a crucial diagnostic tool for quantum thermalization, distinguishing between area-law scaling in localized phases and volume-law scaling in thermalizing regimes consistent with the ETH. In these calculations, to ensure robustness against specific initial conditions and minimize dynamical fluctuations,

averaging was performed over 180 realizations of random product states.

Each realization is represented by a general product state on the Bloch sphere, defined as:

$$|\theta, \phi\rangle = \prod_{i=1}^N \left(\cos \frac{\theta}{2} |Z_+^i\rangle + e^{i\phi} \sin \frac{\theta}{2} |Z_-^i\rangle \right) \quad (3.1)$$

Where ϕ and θ denote the spherical coordinates of the Bloch vector for each spin, and $|Z_+^i\rangle$ and $|Z_-^i\rangle$ represent the eigenstates of the operator σ_i^z (spin-up and spin-down along the z axis). For simplicity, it is assumed that the angles are identical for all sites within a single realization, i.e., $\theta_i = \theta$ and $\phi_i = \phi$ for every i , implying that the system is prepared in a spatially uniform product state. However, the values of θ and ϕ are sampled randomly for each realization to cover different energy densities within the spectrum.

For a system evolving in a general state $|\psi(t)\rangle$, the reduced density matrix of subsystem A is defined as follows:

$$\rho_A(t) = \text{Tr}_B[|\psi(t)\rangle\langle\psi(t)|]. \quad (3.2)$$

where B denotes the complement of subsystem A . This density matrix forms the basis for the calculation of all entanglement measures and encodes the loss of local information due to scrambling. The von Neumann entropy of subsystem A , which quantifies the degree of entanglement between A and B , is defined in the standard form as follows:

$$\mathcal{S}_A(t) = -\text{Tr}(\rho_A(t) \ln \rho_A(t)) \quad (3.3)$$

In integrable systems, such as the local integrable limit of the Ising model $g = 0$, $h_z = 0$, the entanglement entropy grows linearly in time. This ballistic spreading of correlations is governed by the quasiparticle picture and is strictly constrained by the Lieb–Robinson bound [45–48]. However, it is the presence of an extensive set of local conserved charges that prevents true thermalization, restricting the steady-state entropy to sub-thermal values described by a GGE. Consequently, the system exhibits persistent temporal oscillations and non-decaying correlations, and quantum information is transported ballistically via quasiparticles without undergoing chaotic scrambling.

In contrast, in the quantum chaotic regimes induced by nonlocal interactions $g \neq 0$ and/or a longitudinal field $h_z \neq 0$, the system rapidly scrambles quantum information. The entanglement entropy exhibits rapid, volume-law growth, and local observables swiftly relax to a true thermal state consistent with the ETH [22, 49]. In this ergodic phase, the dynamics of multipartite entanglement and operator complexity are markedly accelerated. This rapid scrambling and thermalization serve as the dynamical counterparts to the spectral transition from Poissonian to Wigner-Dyson level statistics.

In nonlocal Ising models, the entanglement velocity v_E is enhanced as the coefficient g or the longitudinal field h_z is increased, while the saturation Time (t_{sat}) is correspondingly reduced:

$$\mathcal{S}_A(t) \approx \begin{cases} v_E t & , t < t_{\text{sat}} \\ \mathcal{S}_{\text{thermal}} & , t \geq t_{\text{sat}} \end{cases} \quad (3.4)$$

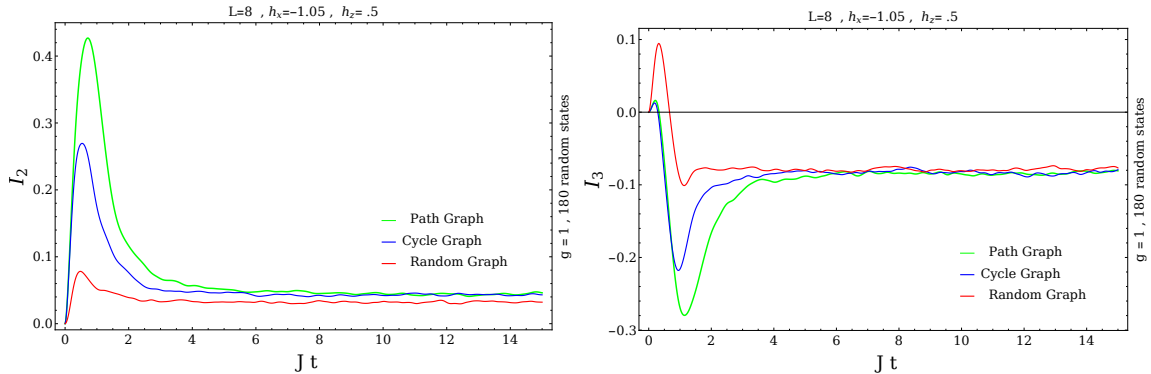


Figure 4. In this figure shows the bipartite (left) and tripartite (right) mutual information computed under the Ising Hamiltonian on a path graph, a cycle graph, and a random graph; the results were averaged over 180 random initial states and plotted as a function of the parameter Jt .

Where $\mathcal{S}_{\text{thermal}}$ denotes the entropy in the thermal state [50]. This behaviour is manifestly related to the analysis of the energy spectrum, the Level spacing distribution, and the presence or absence of conserved quantities, and it emphasises the role of nonlocal interactions and nonintegrability in determining the system’s dynamics [51–53].

Analysis of entanglement entropy growth serves as a fundamental diagnostic parallel to the calculations of OTOC and Krylov complexity, since rapid entanglement spreading and operator growth are directly reflected in the behavior of modern diagnostics of quantum chaos. This framework permits a precise comparison between integrable and non-integrable systems and enables the prediction of their thermalization behavior under varying conditions.

Beyond single-particle measures, the evaluation of mutual information between subsystems constitutes a highly effective tool for probing how quantum information disperses and propagates within a system. The bipartite mutual information, defined as $I(A : B) = S_A + S_B - S_{AB}$, quantifies the total correlations (classical and quantum) shared by two subsystems. It can reveal the temporal formation and decay of local correlations. In systems where quasiparticles are mobile and a finite propagation speed enforces an effective light-cone (bounded by the Lieb-Robinson velocity), the growth of mutual information between spatially separated regions occurs with a delay and increases approximately linearly in time; this growth may be accompanied by oscillations or transient revivals. This feature is observed particularly in integrable systems, where information remains localized within ballistic quasiparticle modes.

By contrast, in chaotic systems governed by the ETH, quantum information is rapidly scrambled across the entire many-body spectrum. Consequently, on short timescales, the mutual information between small local subsystems decays, reflecting the absence of pronounced local revivals. This behavior signifies that local information is swiftly delocalized into highly non-local, global degrees of freedom.

Moreover, the tripartite mutual information, I_3 constitutes a more sensitive probe for

examining the multipartite distribution of information. Defined as $I_3(A : B : C) = I(A : B) + I(A : C) - I(A : BC)$, the sign and magnitude of I_3 serve as a direct diagnostic for information scrambling. In chaotic systems where information is rapidly dispersed across all degrees of freedom, I_3 attains large negative values. This indicates the global delocalization of information and satisfies the monogamy of mutual information. By contrast, in systems close to the integrable limit, I_3 is typically suppressed in magnitude or becomes positive, consistent with the presence of long-lived quasiparticles and the violation of mutual information monogamy due to localized information revivals.

Thus, time-resolved analyses of bipartite and tripartite mutual information, together with entropy and other diagnostics, provide a powerful means to distinguish chaotic dynamics from integrable behavior and yield deep insight into the spreading and redistribution of quantum information in complex systems, ultimately characterizing the route to thermal equilibrium.

To illustrate the foregoing analysis, Fig.4 displays the temporal behavior of the bipartite and tripartite mutual information under Ising Hamiltonians defined on graph-theoretic structures with varying connectivity patterns. The results were averaged over 180 random initial states sampled from the Hilbert space and plotted for different evolution times to ensure statistical robustness and minimize sample-specific fluctuations. This averaging procedure is essential for capturing the typical behavior of the system and for making meaningful comparisons with ETH predictions, which concern the properties of typical eigenstates and initial conditions. The mutual information dynamics shown here provide direct insight into how quantum correlations spread across subsystems and how the system approaches thermal equilibrium in the chaotic regime, while exhibiting persistent oscillations and slower relaxation in the integrable limit.

4 OTOC and chaos diagnostics

In nonequilibrium quantum many-body systems, the characterization of quantum chaos and the propagation of information are of critical importance. One of the principal diagnostics for this analysis is the OTOC. For two Hermitian operators $\hat{V}(0)$ and $\hat{W}(t)$, the OTOC is conventionally defined in the standard form as:

$$C(t) = -\langle [\hat{W}(t), \hat{V}(0)]^2 \rangle \quad (4.1)$$

In the Heisenberg picture, the time-evolved operator is given by $\hat{W}(t) = e^{i\hat{H}t} \hat{W} e^{-i\hat{H}t}$. The expectation value $\langle \cdot \rangle$ is typically taken over the initial state or within a thermal ensemble [54]. The OTOC not only quantifies the decay of operator correlations as a function of time but also characterizes the butterfly velocity at which local perturbations spread and quantum information scrambles across the system. The designation 'Out-of-Time-Order' arises from the non-chronological arrangement of operators within the correlator structure. In particular, if \hat{W} and \hat{V} are both Hermitian and unitary (satisfying $\hat{W}^2 = \hat{V}^2 = \hat{I}$, such as Pauli matrices), the commutator squared simplifies to:

$$C_{WV} = 2(1 - \text{Re}f_{WV}(t)) \quad (4.2)$$

where $f_{WV} \equiv \langle \hat{W}(t) \hat{V} \hat{W}(t) \hat{V} \rangle$.

In systems exhibiting quantum chaos, the $C(t)$ demonstrates exponential growth at early times before saturating:

$$C(t) \sim \epsilon e^{\lambda_L t} \quad (4.3)$$

Here, λ_L denotes the quantum Lyapunov exponent and ϵ represents the magnitude of the initial perturbation. The Lyapunov time, defined as $t_L \sim \frac{1}{\lambda_L}$ provides a characteristic timescale for the rate at which small perturbations spread rapidly throughout the entire system [31, 55–57]. This exponential growth serves as a principal signature of quantum chaos and the onset of operator scrambling, distinguishing chaotic dynamics from integrable behavior.

In integrable systems, the growth of the OTOC is typically non-exponential, often exhibiting polynomial or bounded oscillatory behavior. This reflects constrained information propagation and the absence of genuine quantum chaos, distinguishing it fundamentally from thermalizing systems [58, 59]. This pronounced distinction between integrable and non-integrable dynamics is consistent with the observations reported in Section 2 regarding the saturation values and growth rates of entropy and entanglement.

The relationship between the OTOC, Krylov complexity, and the underlying Krylov space is of central importance for diagnosing operator spreading. In chaotic systems, the exponential growth of the OTOC is directly associated with a linear growth of the Lanczos coefficients, which drives a rapid increase in Krylov complexity and the delocalization of the operator wavefunction within the Krylov basis. In other words, systems characterized by an exponentially growing OTOC facilitate the rapid generation of extensive correlations and operator scrambling [60, 61].

For nonlocal Ising models, the combined presence of nonlocal interactions and a longitudinal field induces an increase in the Lyapunov rate λ_L and a concomitant decrease of the Lyapunov time t_L . This indicates accelerated information scrambling and enhanced entanglement growth, aligning with the mechanisms required for efficient thermalization. These results are fully consistent with the rapid entropy growth and the entanglement-dynamics behavior reported in the previous section [62, 63].

From a spectral perspective, the OTOC is intimately connected to the energy spectrum and the level-spacing distribution. In non-integrable systems adhering to the ETH, spectral statistics transition from Poissonian to Wigner-Dyson distributions. This spectral complexity and energy level repulsion give rise to an increased Lyapunov rate and accelerated operator spreading, which is compatible with rapid entropy growth and the efficient spreading of quantum information across the Hilbert space.

By means of this framework, a precise analysis of nonequilibrium quantum systems (both integrable and chaotic) is made possible. Consequently, the groundwork is laid for advanced investigations of Krylov complexity as a diagnostic tool, spectral statistics, and other contemporary measures of quantum chaos and thermalization in the subsequent sections. As shown in Fig. 5, in graph-based Ising models defined on random graphs and on the path graph (where the system exhibits chaotic dynamics) an initial exponential growth is clearly observed. Following the scrambling time, the correlator relaxes toward

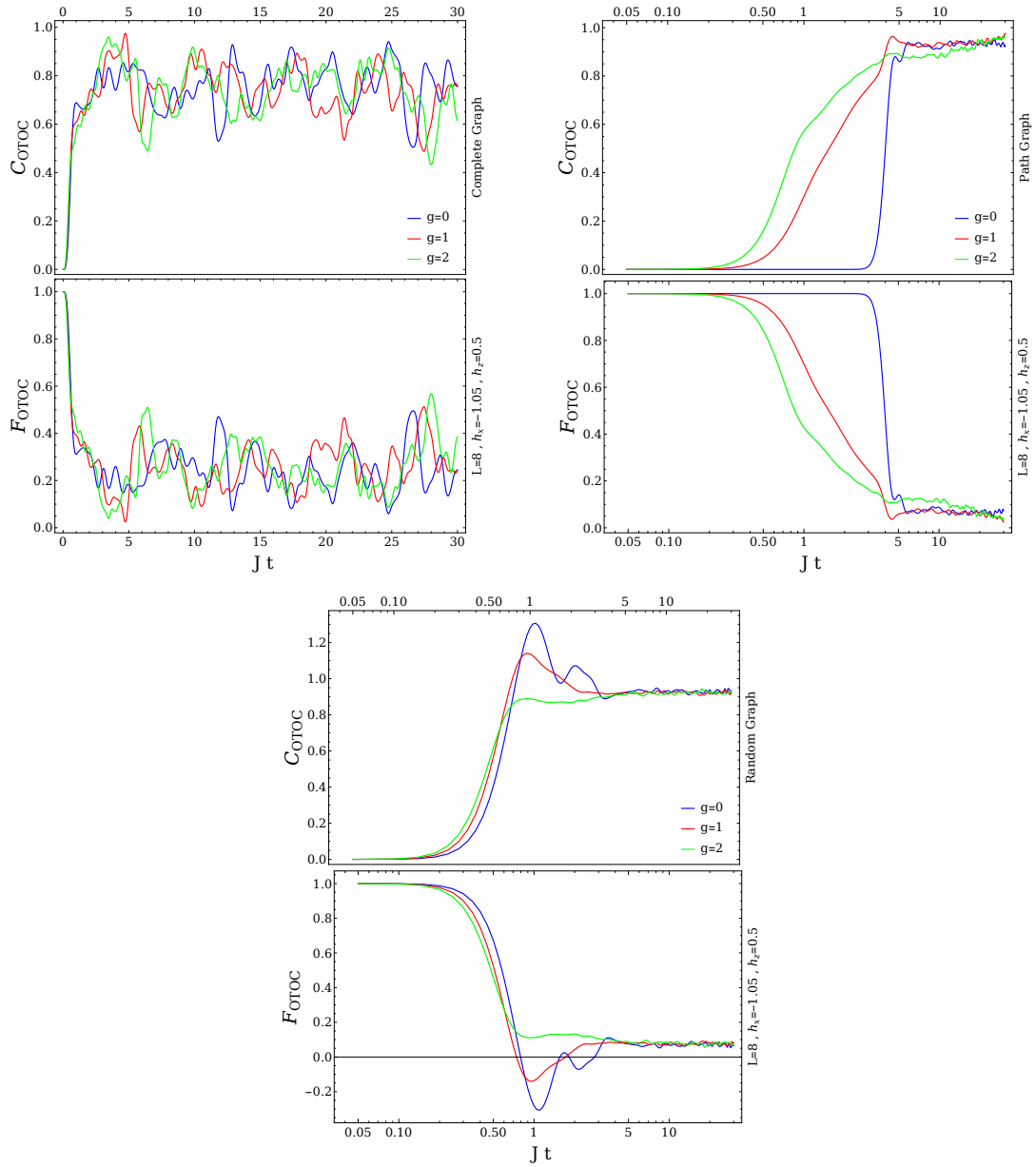


Figure 5. In each of the above plots, the time evolution of the OTOC (upper panel of each plot) and of the function f_{WV} (lower panel of each plot) have been computed and displayed.

a steady state. As expected for these chaotic systems, late-time coherent oscillations are strongly suppressed, and the OTOC saturates at an approximately constant value, signaling complete operator scrambling.

5 Krylov complexity, spectral diagnostics of chaos, and their connection to entanglement

Operator complexity, particularly Krylov complexity, provides a rigorous framework for characterizing the growth of local operators in nonequilibrium, chaotic quantum systems. This diagnostic is intrinsically linked to information scrambling and the propagation of entanglement in multipartite systems, serving as a dynamical precursor to thermalization. Krylov complexity is defined within the operator space spanned by the orthonormal Krylov basis vectors $|\mathcal{O}_n\rangle$, quantifying the spreading of the operator $|\mathcal{O}(t)\rangle$ under time evolution:

$$|\mathcal{O}(t)\rangle = e^{i\hat{L}t}|\mathcal{O}_0\rangle = \sum_{n=0}^{\infty} \phi_n(t)|\mathcal{O}_n\rangle, \quad \sum_n |\phi_n(t)|^2 = 1 \quad (5.1)$$

Krylov complexity is defined as the expectation value of the basis index n :

$$K(t) = \sum_{n=0}^{\infty} n |\phi_n(t)|^2 \quad (5.2)$$

which quantifies the degree of "operator spreading in Krylov space." A rapid growth of $K(t)$ signals high operator complexity, fast information propagation, and pronounced quantum chaos [64–68].

The Lanczos coefficients b_n , which tridiagonalize the Liouvillian \hat{L} in Krylov space, play a central role in determining $K(t)$.

$$\hat{L}|\mathcal{O}_n\rangle = b_{n+1}|\mathcal{O}_{n+1}\rangle + b_n|\mathcal{O}_{n-1}\rangle, \quad n \geq 0, \quad b_0 = 0 \quad (5.3)$$

The asymptotic behavior of b_n constitutes a key diagnostic for distinguishing between integrable and chaotic regimes, often referred to as the Universal Operator Growth Hypothesis. In integrable systems, b_n remains bounded or increases only slowly, and consequently $K(t)$ exhibits slow or oscillatory growth. In chaotic systems, $b_n \sim \alpha n + \gamma$ (for $n \gg 1$) grows linearly, leading to an exponential increase in $K(t)$ up to the saturation regime, consistent with the onset of thermalization and ETH [69–71].

The behavior of the Lanczos coefficients b_n across different graph geometries provides a powerful diagnostic tool for distinguishing integrable from chaotic quantum dynamics. As illustrated in Figures 6 and 7, the extent of the Lanczos sequence n directly reflects the dimensionality of the Krylov subspace explored by the time evolution. For the complete graph, the dynamics are confined to a dramatically reduced subspace with $n \approx L$, a hallmark of integrable mean-field models where conservation laws restrict the accessible phase space. In stark contrast, the random graph geometry induces chaotic scrambling, forcing the Lanczos algorithm to explore an exponentially large Krylov subspace with $n \approx 2^L$. This saturation of Krylov complexity signifies that the initial state $|Y+\rangle$ has effectively delocalized across the entire Hilbert space, a defining feature of quantum chaotic systems. The intermediate behavior observed in the cycle and path graphs suggests partial symmetry breaking, where the dynamics access larger subspaces than the complete graph but do not achieve full Hilbert space exploration, consistent with their quasi-integrable

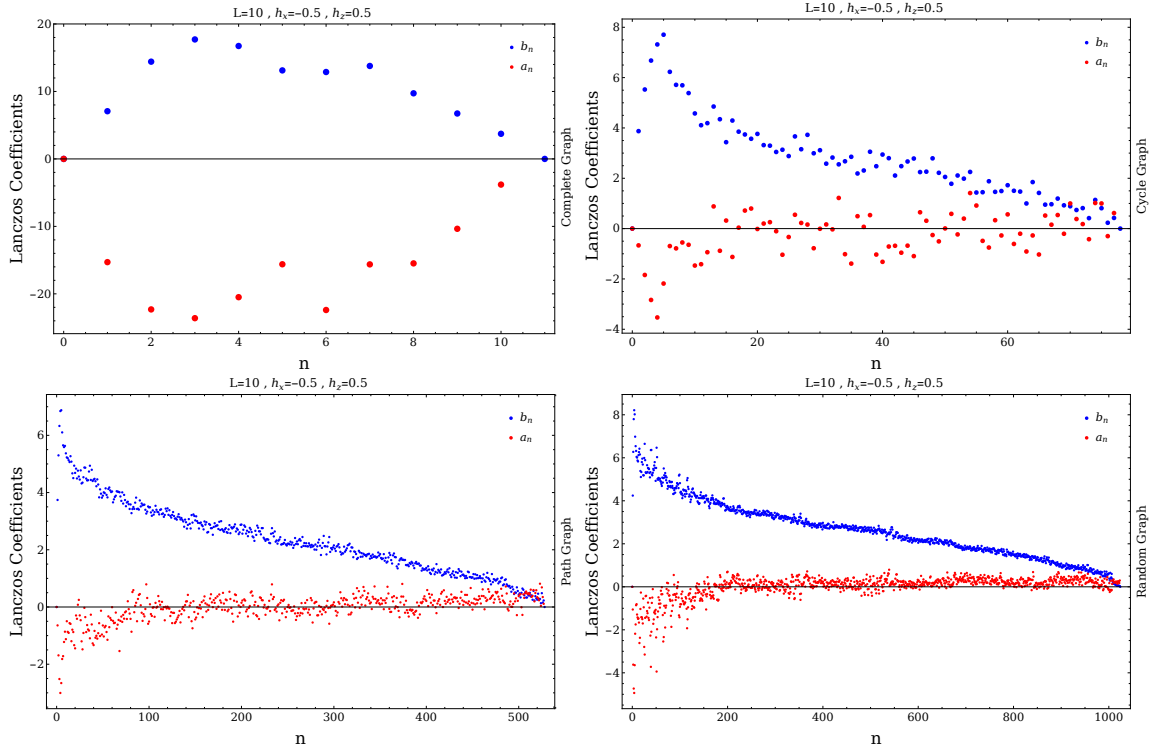


Figure 6. In this figure, the Lanczos coefficients are plotted as a function of n for the Ising model. The calculations were performed with parameters $h_x = -0.5$, $h_z = 0.5$, and $L = 10$, and the following graph geometries were employed: the complete graph (top-left), the cycle graph (top-right), the path graph (bottom-left), and the random graph (bottom-right). It should be noted that the initial state $|Y+\rangle$ was used in the computation and plotting of these panels.

nature. The connection between Krylov complexity and measures of entanglement and entropy is theoretically well-founded, with growing evidence for experimental accessibility. If the system is partitioned into two subsystems, A and B , the von Neumann entropy of subsystem A is defined as follows:

$$\mathcal{S}_{vN}(\rho_A) = -\text{Tr}[\rho_A \log \rho_A] \quad (5.4)$$

where ρ denotes the density matrix of the full system. In chaotic, non-integrable systems adhering to ETH, the rapid growth of $K(t)$ is concomitant with a simultaneous increase of the von Neumann entropy \mathcal{S}_{vN} and multipartite entanglement. This occurs because local operators rapidly explore the entire Hilbert space and scramble information across different parts of the system [72–74]. This observation establishes a precise physical connection between Krylov complexity and entanglement dynamics, complementing diagnostics such as OTOCs and entropy growth in characterizing thermalization.

From a spectral perspective, the interplay between the Lanczos coefficients b_n and the structure of the system’s energy spectrum is fundamental. Nonintegrable systems, which exhibit Wigner–Dyson statistics consistent with the ETH, typically display rapidly growing b_n ; this leads to exponential increases in Krylov complexity $K(t)$ and von Neumann

entropy S_{vN} . By contrast, integrable systems characterized by Poissonian spectra feature slow growth of b_n , resulting in $K(t)$ showing linear or otherwise limited growth [75, 76]. Moreover, the time-dependent distribution $|\phi_n(t)|^2$ in the Krylov basis and its moments are intrinsically related to the autocorrelation function of the initial operator, defined as:

$$(\mathcal{O}_0|\mathcal{O}(t)) = \phi_0(t) \quad (5.5)$$

All of these quantities are consistent with the behaviour of entanglement entropy and align with the temporal evolution of the OTOC, serving as proxies for information scrambling [65, 73].

For nonlocal Ising models, the addition of nonlocal interactions and a longitudinal field results in an enhancement of the Lyapunov rate λ_L , rapid growth of the Lanczos coefficients b_n , and significant increases in $K(t)$ and the von Neumann entropy S_{vN} ; this behavior indicates faster information scrambling and more extensive entanglement spreading. Numerical studies in the early-time scrambling regime have demonstrated a quantitative relation between the growth rate of Krylov complexity and the initial slope of the von Neumann entropy, such that an approximate proportionality between these quantities: $\frac{dk}{dt} \propto \frac{dS_{vN}}{dt}$ is observed. Accordingly, Krylov complexity can be employed as an alternative or complementary diagnostic for entanglement growth and thermalization dynamics [77].

Finally, complementary diagnostics, such as the Inverse Participation Ratio (IPR) in Krylov space, the average ratio of consecutive level spacings, and the SFF, furnish a comprehensive picture of chaotic dynamics and entanglement. When these diagnostics are considered together with $K(t)$ and S_{vN} , a precise discrimination between integrable and chaotic regimes, and between local and nonlocal systems, is enabled. This multi-faceted approach establishes a quantitative link between operator growth, the validity of ETH, and the spreading of quantum information [78, 79].

To investigate the dynamical behavior of Krylov spread complexity, one may study the temporal evolution of the expectation value of the Krylov number operator. This expectation value, particularly in the long-time limit, constitutes a robust diagnostic for identifying the chaotic character of a given system and probing the onset of thermalization. By expanding the initial state in the energy eigenbasis as $|\psi_0\rangle = \sum_{j=1}^{D_\psi} c_j |E_j\rangle$, the complexity can be rewritten in the following spectral decomposition form:

$$K(t) = Tr(\rho_{DE}N) + \sum_{j \neq k}^{D_\psi} e^{i\omega_{jk}t} c_j^* c_k N_{jk} \quad (5.6)$$

where $N = \sum_{n=0}^{D_\psi-1} n |n\rangle \langle n|$ is the number operator in the Krylov basis. Moreover, in the above relations $\omega_{jk} = E_j - E_k$, $N_{jk} = \langle E_j | N | E_k \rangle$, and ρ_{DE} denotes the diagonal ensemble density matrix, which is defined as follows:

$$\rho_{DE} = \sum_{j=1}^{D_\psi} |c_j|^2 |E_j\rangle \langle E_j| \quad (5.7)$$

It is crucial to note that, when starting from the initial state, we restrict our attention to a single fixed-charge sector of the full Hilbert space. The Krylov subspace is consequently

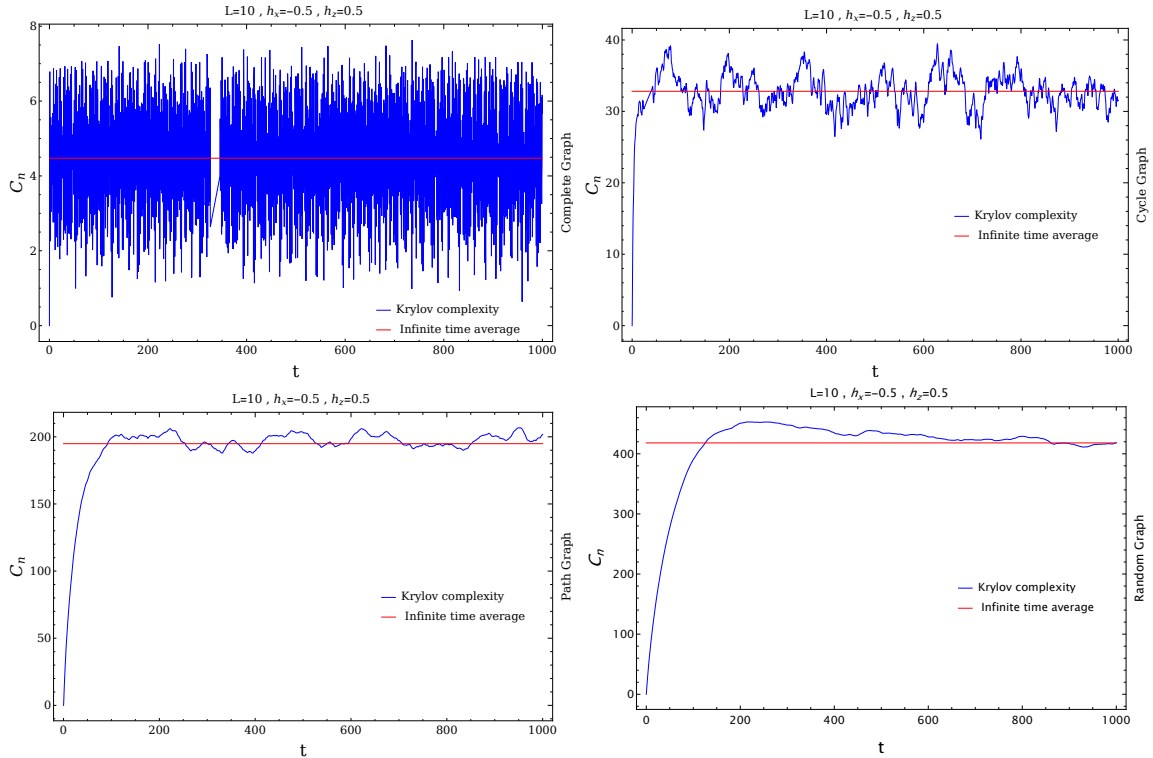


Figure 7. Complexity growth for the Ising models defined on graphs is shown for the following geometries: the complete graph (top-left), the cycle graph (top-right), the path graph (bottom-left), and the random graph (bottom-right). The red line in the plots denotes the infinite-time-averaged Krylov complexity. It should be noted that the initial state $|Y+\rangle$ was employed in the computation and plotting of these curves.

constructed within this symmetry block, and accordingly, the diagonal density matrix ρ_{DE} defined above is restricted to that specific sector. In the context of the ETH, the off-diagonal terms in Eq. 5.6 are expected to dephase rapidly for chaotic systems, causing the complexity to saturate. Furthermore, the infinite-time average of the complexity, which reflects the equilibrium value in the thermalized regime, is given by:

$$\bar{K} = \lim_{T \rightarrow \infty} \frac{1}{T} \int_0^T \langle N(t) \rangle dt = \text{Tr}(\rho_{DE} N) \quad (5.8)$$

The saturation value of Krylov complexity and the manner in which it saturates in finite many-body systems can be employed as a robust diagnostic of the system's integrable or chaotic nature. Within the Krylov basis, where the complexity is defined as the expectation value of the position operator \hat{N} , the long-time saturation value K_s is governed by the Diagonal Ensemble ρ_{DE} . In other words, one may observe at saturation that:

$$\begin{cases} K_s \approx \text{Tr}(\rho_{DE} N) & \text{For a chaotic system} \\ K_s < \text{Tr}(\rho_{DE} N) & \text{For an integrable system} \end{cases} \quad (5.9)$$

This distinction arises because chaotic systems satisfying the ETH explore the available Krylov subspace more uniformly, whereas integrable systems are constrained by conserved

quantities. It should also be noted that, for certain initial states in a chaotic system, the complexity prior to saturation may exhibit a pronounced peak or overshoot before settling to its steady-state value. For a clearer illustration of this behavior, see Fig.7.

Therefore, Krylov complexity, when analyzed alongside spectral and entanglement-based diagnostics, furnishes a comprehensive and rigorous framework for the study of nonequilibrium quantum systems. This framework is applicable both at the theoretical level and in numerical simulations, and it is closely connected to the OTOC and entropy growth through the underlying mechanism of operator scrambling. This unified perspective enables a detailed investigation of local and nonlocal Ising systems, distinguishes between integrable and chaotic regimes via ETH signatures, and facilitates the prediction of the long-time behaviour of entanglement and operator complexity.

6 Spectral diagnostics of chaos, the SFF, and their connection to entanglement growth and operator complexity

Spectral analysis of quantum systems, viewed from the standpoint of statistical properties and energy correlations, constitutes one of the most fundamental approaches for detecting and quantifying quantum chaos.

In closed quantum systems with a discrete energy spectrum $\{E_n\}$, ordered as $E_1 < E_2 < \dots$, one of the simplest and most widely used diagnostics is the distribution of consecutive level spacings $s_n = E_{n+1} - E_n$. For a meaningful comparison between different systems, the spectrum must be unfolded so that the local spectral density is normalized to unity. After unfolding, RMT predicts that, for chaotic (nonintegrable) systems possessing time-reversal symmetry, the level-spacing distribution assumes the Wigner-Dyson form characteristic of the GOE.

(For example, for the GOE):

$$P_{WD}(s) = \frac{\pi}{2} s \exp\left(-\frac{\pi}{4} s^2\right) \quad (6.1)$$

Whereas integrable systems are typically characterized by Poissonian level-spacing statistics:

$$P_{Pois}(s) = e^{-s} \quad (6.2)$$

To quantify this more efficiently and without the need to perform a full spectral unfolding, the consecutive gap ratios r_n are defined as:

$$r_n = \frac{\min(s_n, s_{n-1})}{\max(s_n, s_{n-1})}, \quad \langle r \rangle = \frac{1}{N-2} \sum_{n=2}^{N-1} r_n \quad (6.3)$$

The mean value $\langle r \rangle$ is approximately 0.386 for a Poissonian spacing distribution and approximately 0.531 for the GOE; accordingly, $\langle r \rangle$ constitutes a simple and robust diagnostic for distinguishing integrable and chaotic regimes [80, 81]. Crucially, the emergence of Wigner-Dyson statistics in the spectrum is deeply connected to the validity of the ETH, as it signals the absence of extensive conserved quantities that would otherwise prevent thermalization.

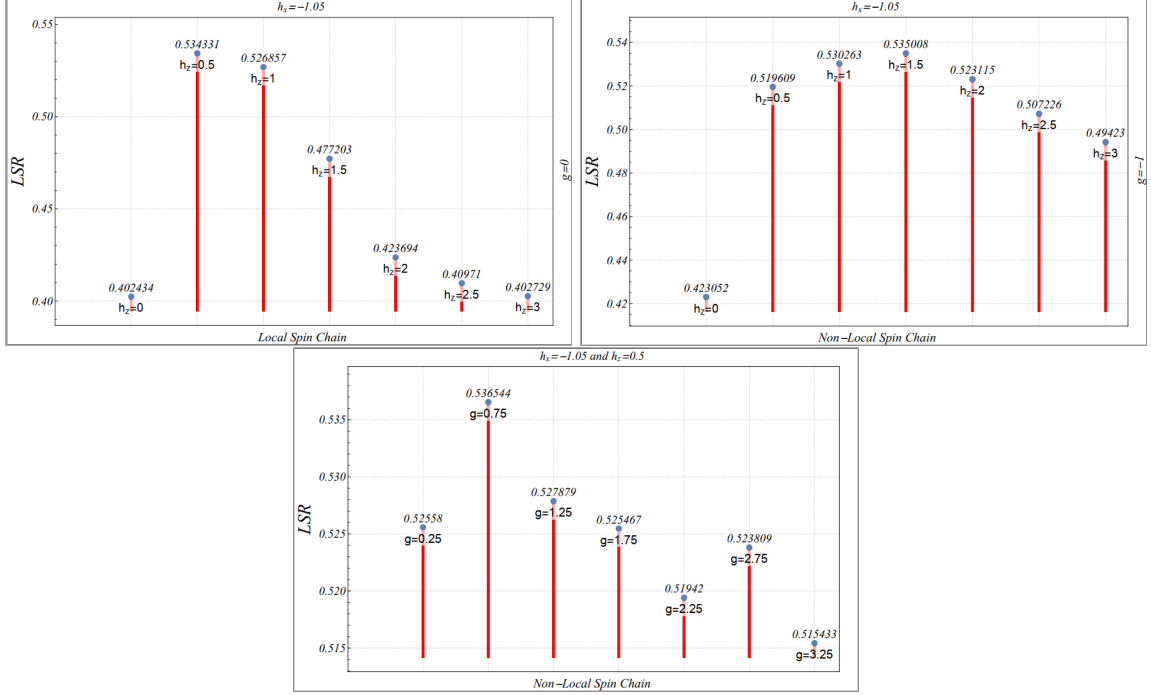


Figure 8. The panels display the ratios of adjacent energy-level spacings in the Ising model with a mixed field and nonlocal interactions. The top-left panel shows the distribution of spacing ratios for the Ising model with a transverse field $g = 0$ under various values of the longitudinal field h_z . The top-right panel presents results for the Ising model with a mixed field at fixed $g = -1$ and varying h_z . The bottom panel displays the distribution of spacing ratios for fixed $h_z = 0.5$ as the strength of the nonlocal interaction g is varied.

These diagnostics play a direct and crucial role in the spectral analysis of both local and nonlocal Ising chains. Specifically, the introduction of integrability-breaking perturbations, such as a longitudinal field or nonlocal interactions, typically shifts $\langle r \rangle$ from its Poissonian value toward that of the GOE. This spectral crossover signifies the transition from an integrable regime to a chaotic one, marking the onset of eigenstate thermalization consistent with the ETH [80, 82].

As shown in Fig. 8, for $|g| \geq 0.25$ the system's chaotic behavior is clearly observed, marking the transition from integrable to non-integrable dynamics. Moreover, for the local Ising model with $h_x = -1.05$, chaotic dynamics are realized for $h_z = 0.5$, whereas the system remains integrable for $h_z = 0$. These findings are corroborated by the corresponding Krylov complexity plots, which exhibit exponential growth in the chaotic regime consistent with operator scrambling.

Given that level-spacing statistics provide a local, short-range diagnostic of the energy spectrum, the analysis of dynamical behavior and temporal spectral correlations requires measures that also capture information on longer spectral scales. The SFF serves as a premier diagnostic in this context, being intimately connected to the system's return probability (or analytically continued partition function) and highly sensitive to the global spectral rigidity that underpins quantum thermalization. The standard definition of the

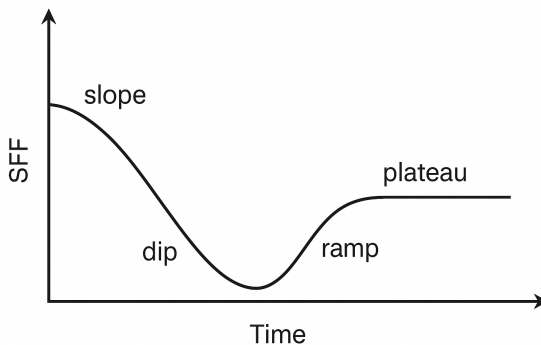


Figure 9. Schematic diagram of the SFF for chaotic systems, exhibiting four distinct regimes: the slope, the dip, the ramp, and the plateau.

SFF at inverse temperature β is given by:

$$SFF(\beta, t) = |Z(\beta + it)|^2 = Z(\beta + it)Z(\beta - it), \quad Z(\beta) = \text{Tr} e^{-\beta \hat{H}}. \quad (6.4)$$

The SFF encodes two-level energy correlations and the spectral time scales over which the system exhibits the universal behavior characteristic of RMT. The temporal structure of the SFF is typically separable into four distinct regimes:

1. **Initial Slope:** The initial decay of the SFF at very short times, reflecting the single-particle density of states and non-universal features of the spectrum.
2. **Dip:** Occurring prior to the onset of the linear ramp, indicative of intermediate-range spectral correlations and the formation of the correlation hole.
3. **Linear Ramp:** A linear increase indicative of long-range spectral correlations and spectral rigidity characteristic of Wigner-Dyson statistics; this regime is a prerequisite for ETH.
4. **Plateau (Saturation):** The late-time regime in which the SFF attains a constant value; this regime is associated with the Heisenberg time t_H , defined as the inverse of the mean level spacing, marking the onset of quantum recurrence.

In realistic chaotic systems, the emergence of an initial slope, a dip, a linear ramp, and a plateau constitute clear signatures of spectral correlations characteristic of RMT; this behavior is clearly visible in Fig. 10. By contrast, in integrable systems governed by Poissonian statistics, the linear ramp is absent or significantly suppressed, and the saturation behavior differs fundamentally, reflecting the lack of level repulsion and the absence of complete information scrambling [83–85]. Within the analysis of spectral correlations via the SFF, two spectral time scales are of particular importance: the Thouless time t_{Th} and the Heisenberg time t_H . The Heisenberg time t_H can be approximately defined as: $t_H \sim \frac{2\pi}{\overline{\Delta E}}$. Here $\overline{\Delta E}$ denotes the mean energy spacing within a window of the spectrum. t_H represents the timescale required for effects associated with the discrete (quantized) nature of

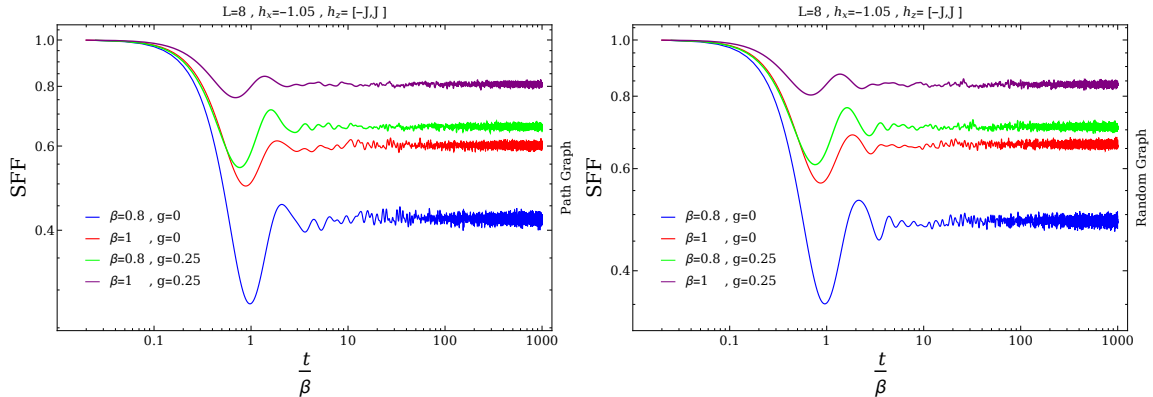


Figure 10. The SFF of the Ising model on the path graph and on the random graph has been computed and plotted as a function of the parameter $\frac{t}{\beta}$.

the spectrum — i.e., the resolution of individual level spacings — to become manifest; consequently, the SFF plateau emerges on this timescale, signaling the saturation of spectral correlations. The Thouless time t_{Th} provides a measure of the time required for the system to attain universal RMT behavior, marking the onset of the ramp in the SFF. Physically, t_{Th} is often identified with the thermalization time scale in the context of the ETH. In local systems, t_{Th} is typically related to transport properties and operator spreading and can be significantly shorter than t_H , often scaling polynomially with system size. By contrast, in systems with nonlocal interactions and rapid entanglement growth (fast scrambling), t_{Th} is appreciably reduced, potentially scaling logarithmically with the Hilbert space dimension, causing the SFF to reach the ramp and plateau more rapidly [86].

The relationship between spectral measures and entanglement constitutes one of the central points of this section and is of considerable significance from both physical and mathematical viewpoints. Several key relations and an important line of reasoning can be highlighted here:

- A. The SFF, which encodes pairwise correlations of energy levels, signifies "spectral scrambling"; when the SFF reaches the ramp and plateau, the spectra of operators exhibit random-matrix-like behavior in accordance with the predictions of RMT. This spectral randomization typically coincides with rapid entanglement growth: that is, in regimes where the SFF rapidly attains the ramp and the Thouless time t_{Th} is short, faster increases of the von Neumann entropy S_{vN} and more rapid saturation to the thermal (or corresponding equilibrium) value are generally observed. Hence, t_{Th} may be regarded as a characteristic time for the onset of the system's effective processes and for the commencement of rapid entropy growth [87].
- B. Semi-quantitative and empirical relations can be established between spectral timescales and parameters characterizing entropy growth and OTOC. For instance, the entropy saturation time t_{sat} is generally found to correlate strongly with t_{Th} , while being bounded from above by the Heisenberg time t_H . For systems with $t_{Th} \ll t_H$ — i.e.,

systems that rapidly attain universal RMT behavior — t_{sat} is located close to or slightly above t_{Th} ; whereas for systems proximate to integrability, t_{Th} is ill-defined or extremely large and t_{sat} is correspondingly significantly larger [88]. Physically, this implies that complete operator spreading and the uniform redistribution of information across subsystems do not occur until the spectrum exhibits sufficiently strong long-range correlations.

- C. The entanglement energy spectrum, and in particular the properties of the eigenvalue spectrum of the reduced density matrix, play an important role in elucidating this connection. The eigenvalue spectrum of ρ_A not only determines entropy values, but the spectral structure of these eigenvalues can serve as a "spectral mirror" of the system's underlying dynamics. If the level spacing statistics of the reduced eigenvalue spectrum follow Wigner-Dyson distributions, this indicates that the subsystems are effectively thermalized and that operators distribute information randomly among the subsystems. This scenario is consistent with large values of the SFF in the ramp regime and with exponential growth of the OTOC [89–92].
- D. From the perspective of the ETH, eigenstate thermalization constitutes a fundamental concept for understanding how isolated quantum systems evolve toward thermal equilibrium. Despite the deterministic and unitary nature of quantum mechanics, ETH explains that nonintegrable quantum systems may thermalize without coupling to an external environment. The central idea is that the energy eigenstates of such systems can reproduce expectation values identical to those of thermal equilibrium states, governed by smooth functions of energy. Modern formulations of ETH therefore posit that, for nonintegrable quantum systems, individual energy eigenstates act effectively as thermal states. This stance marks a departure from classical statistical mechanics, in which thermalization requires the exploration of the full set of accessible microstates via ergodic trajectories.

This hypothesis postulates that the expectation value of a measurable quantity in any energy eigenstate $|n\rangle$ with energy $E_n \approx E$ approaches the corresponding thermal expectation value at energy E . Mathematically, the matrix elements of the observable operator \hat{O} between the eigenstates $|m\rangle$ and $|n\rangle$ are expressed as:

$$O_{mn} = \langle m|\hat{O}|n\rangle = \bar{O}(E)\delta_{mn} + e^{-S(E)/2}f(E,\omega)R_{mn} \quad (6.5)$$

where $\bar{O}(E)$ denotes the thermal expectation value of \hat{O} at energy E , $S(E)$ is the entropy at energy E , and $f(E,\omega)$ is a smooth function with ω typically representing the energy difference between levels. The terms R_{mn} are pseudo-random variables with zero mean and unit variance, typically drawn from a Gaussian distribution, subject to the Hermiticity constraint $R_{mn} = R_{nm}^*$. Fig. 11 displays the matrix representation of the observable S_x in the eigenstate basis $|n\rangle$ of the Ising Hamiltonian, where the matrix elements $\langle m|S_x|n\rangle$ are plotted as a function of eigenstate indices m and n for both a random graph (left) and a Watts–Strogatz small-world network (right), with parameters $h_x = 0.5$, $h_z = 1$, and $L = 11$. The matrix structure reveals the key predictions of the ETH. The diagonal elements

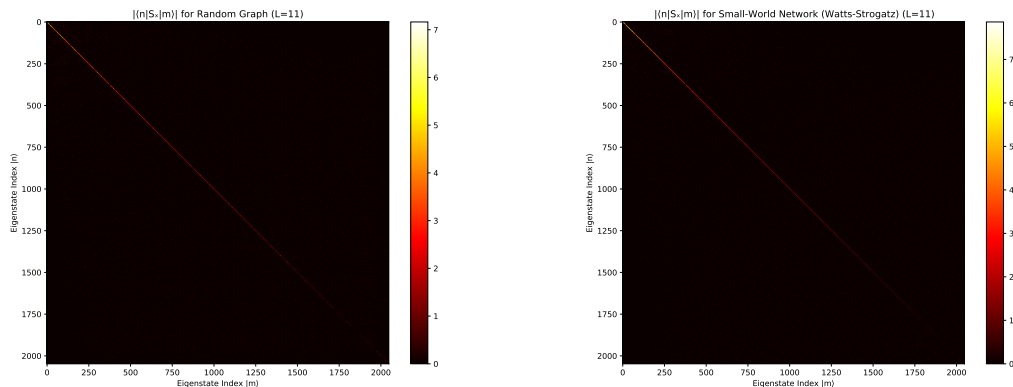


Figure 11. Matrix elements $\langle m|S_x|n\rangle$ of the spin operator S_x in the energy eigenbasis $\{|n\rangle\}$ of the Ising Hamiltonian, plotted as a function of eigenstate indices m and n . Left panel: random graph; right panel: Watts–Strogatz small-world network. System parameters are $h_x = 0.5$, $h_z = 1$, and $L = 11$. The matrix structure demonstrates the fundamental ETH ansatz: the diagonal elements $\langle n|S_x|n\rangle$ (bright line along the main diagonal) vary smoothly as a function of the eigenstate index, corresponding to a smooth function of energy $O(E_n)$. The off-diagonal elements $\langle m|S_x|n\rangle$ for $m \neq n$ are exponentially suppressed in the system size, appearing as the dark background, consistent with the ETH scaling $e^{-S/2} f(E, \omega) R_{mn}$. The nearly identical structure in both network topologies indicates that ETH is satisfied independently of the underlying graph structure.

$\langle n|S_x|n\rangle$ (visible as the bright line along the main diagonal) exhibit smooth variation with eigenstate index, forming a slowly varying function of energy as required by ETH. In contrast, the off-diagonal elements $\langle m|S_x|n\rangle$ for $m \neq n$ are exponentially suppressed, appearing as the dark background throughout the matrix.

The exponential suppression factor $e^{-s(E)/2}$ ensures that off-diagonal matrix elements are exponentially small in the system size, thereby guaranteeing that long-time averages of observables converge to thermal values despite the unitary evolution. Modern formulations of the ETH are most applicable to non-integrable systems, where quantum chaos plays a central role. In integrable systems, which possess an extensive number of conserved quantities, eigenstates exhibit an ordered, non-chaotic structure and, consequently, thermalization to the Gibbs ensemble does not occur; instead, such systems typically relax to a GGE. It is worth noting that a distinct mechanism for the violation of ETH arises in disordered systems exhibiting Many-Body Localization (MBL), where ergodicity is broken due to localization rather than integrability.

The ETH ansatz indicates that the off-diagonal components of the operator—which are responsible for information spreading and the growth of the OTOC—depend directly on the spectral function $f_O(\bar{E}, \omega)$ and on the spectral structure of the Hamiltonian. Recent studies have shown that the properties of the SFF and spectral correlations are intrinsically linked to dynamical rates such as the Lyapunov exponent λ_L , and consequently affect the growth rate of entropy and Krylov complexity [18, 82]. In other words, modern formulations of the ETH formally articulate the connection between the energy spectrum,

operator matrix elements, and the process of thermalization; this constitutes precisely the conceptual loop that links the SFF, the OTOC, and entropy.

It should be emphasized that the foregoing analyses, in practice, require numerical care and explicit consideration of finite-size effects. In finite systems the ramp may not fully develop, and the spectral time scales can be perturbed by boundary effects and statistical fluctuations; therefore, direct comparison with RMT must be accompanied by finite-size scaling analysis so that the results can be meaningfully extrapolated to the thermodynamic limit [37, 86, 93–95].

In summary, spectral measures, from level-spacing statistics and the r -ratio to the SFF and multi-level correlation functions, possess substantial analytical and predictive value in the study of non-equilibrium dynamics. These measures not only diagnose the dynamical regime (integrable versus chaotic), but recent studies have indicated that they may serve as indicators for the time scales associated with entanglement spreading, the onset of information scrambling, and the growth of operator complexity. The mathematical link between modern formulations of the ETH, the spectral components of operators, and spectral diagnostics provides a theoretical framework that can be tested in models such as the local and nonlocal Ising models and validated through numerical simulations and experimental measurements.

7 Conclusion

This work establishes a coherent framework for investigating the transition from integrable regimes to quantum chaos by combining a local quantum Ising model with added nonlocal terms and by performing analyses on various graph topologies. The proposed model and accompanying simulations demonstrate that strengthening the nonlocal interactions (parameter g) and applying a longitudinal field h_z drive the system’s spectral properties from distributions close to Poisson toward those consistent with Wigner–Dyson statistics. This spectral transition coincides with a more rapid growth of the von Neumann entropy and with reduced saturation times, signaling the onset of thermalization consistent with the ETH.

An analysis of information-theoretic measures indicates that bipartite and tripartite mutual information play a strong diagnostic role in distinguishing different dynamical regimes: significantly negative values of the tripartite mutual information signal a highly delocalized and effectively irretrievable distribution of information (scrambling), whereas vanishing or near-zero values indicate information accessibility or proximity to integrable behavior. OTOCs likewise exhibit an initial exponential growth characterized by a quantum Lyapunov rate, λ_L which is enhanced with increasing g and h_z ; therefore, OTOCs show strong consistency with spectral and entropic diagnostics in identifying the chaotic phase.

From an operator-centric viewpoint, Krylov complexity and the Lanczos coefficients furnish a microscopic description of the operator-spreading process. The linear growth of the Lanczos coefficients with the basis index, characteristic of the chaotic regime, induces a rapid redistribution of weight over the Krylov basis and a concomitant exponential in-

crease in Krylov complexity at early times. The relation between the Lanczos structure and Krylov complexity therefore provides a quantitatively rigorous means to discriminate between dynamical regimes, further corroborating the connection between operator growth and quantum thermalization.

Spectral diagnostics, including the SFF, the average adjacent-level spacing ratio $\langle r \rangle$, and related measures, provide an independent and consistent framework for identifying the transition to chaos. In particular, the observation of the characteristic "slope–dip–ramp–plateau" structure in the SFF, alongside the shift of the mean $\langle r \rangle$ from the Poisson value toward that of the GOE, corroborates the emergence of long-range spectral correlations inherent to the chaotic regime.

These results indicate that quantum chaos is not merely a spectral property but a multidimensional process arising from the synergistic interplay of local and nonlocal correlations, interaction topology, and operator dynamics. Demonstrating that the time scales of entropy growth, the quantum Lyapunov exponent λ_L , and the growth pattern of Lanczos coefficients converge within a common regime contributes to a deeper understanding of the relationship between the mechanisms of the ETH, information scrambling, and spectral statistics.

A coherent and reliable picture of quantum dynamics is established by the convergence of results obtained from different viewpoints—spectral, information-theoretic, operator-based, and entanglement diagnostics. Such consistency permits chaos or integrability to be diagnosed not by a single indicator but by a "multifaceted profile", which is markedly more precise and robust. Moreover, this theoretical framework can inform practical experimental pathways on platforms such as Rydberg-atom arrays, trapped-ion systems, and photonic architectures.

Accordingly, the results of the present study may bridge the gap between theory and experiment, thereby enabling the direct probing of complex thermalizing behaviors.

It is demonstrated that quantum chaos arises from the interplay between dynamical parameters and the underlying graph architecture.

Network topology acts as a structural encoder that dictates the system's behavior and, through its deformation or inhomogeneity, can steer the dynamics toward integrability or chaos. This insight is not only of significance to fundamental physics but also has direct applications in the design of controllable quantum systems, quantum information protocols, and the development of architectures for quantum information processing.

Future Research Directions

To advance this research frontier, several pivotal directions are proposed. The primary avenue involves developing analytical frameworks that elucidate the role of graph topology in quantum chaos through rigorous derivations. It is essential to establish quantitative relations between structural graph features—such as spectral dimension and connectivity—and chaotic indicators, including the Lyapunov exponent and the tripartite mutual information. Such a formulation would enable the prediction of chaos transition regimes based solely on topological properties, bypassing computationally expensive numerical simulations.

The second avenue entails extending the numerical analysis to larger scales. Simulations must be performed for larger system sizes and a broader variety of graph topologies to disentangle finite-size effects from the intrinsic characteristics of chaos. Finite-size scaling analysis should be employed to identify size-independent critical points and delineate precise boundaries between chaotic and integrable regimes in the thermodynamic limit. Moreover, a systematic comparison among regular, random, small-world, and scale-free graphs is required to construct a comprehensive atlas of dynamical behavior as a function of topology.

The third avenue concerns the investigation of disorder effects within the topology. The introduction of disorder or inhomogeneity in the bonds or fields can shift the boundaries of chaos and may lead to the emergence of phases analogous to MBL. This line of inquiry can elucidate how topological disorder modifies the balance between integrability and chaos, and specifically, how it impacts the validity of the ETH and the propagation of quantum information.

On the other hand, the fourth direction focuses on experimental realization and validation. The design of protocols for implementing specific topologies in experimental platforms—such as the simulation of small-world graphs in Rydberg-atom arrays or the construction of photonic networks with scale-free architectures—would enable the direct observation of the effect of topology on chaos and thermalization dynamics. Such experiments, in addition to providing theoretical validation, would pave the way for the practical exploitation of these phenomena in quantum technologies.

The fifth avenue concerns methodological improvement. Lanczos computations and Krylov complexity measures should be standardized to ensure numerical stability and accuracy, particularly in the presence of finite-size effects. The development of error-resilient algorithms and the release of reference codes and datasets will assist the community in achieving reproducible findings. Furthermore, machine-learning tools may be employed to automate the classification of topologies according to their degree of chaos and adherence to the ETH. Such tools would accelerate the analysis pipeline and yield initial predictions that can guide future research directions.

Finally, the sixth avenue should be devoted to interdisciplinary applications. The results of this study can be directly employed in the design of quantum information-processing systems. Regular graphs may serve as platforms for enhanced control and chaos suppression, whereas complex and heterogeneous graphs can be exploited to enhance security and to render information effectively irreversible via scrambling in quantum cryptographic protocols. Furthermore, connecting these findings to holographic theories and Lyapunov bounds may open a new chapter in linking networked quantum systems with gravitational-holographic descriptions.

Overall, the continuation of this research program should pursue three concurrent thrusts: (1) deepening theoretical and numerical analyses to elucidate the relationship between topology, chaos, and thermalization; (2) designing and implementing experimental protocols for the direct observation of these phenomena; and (3) exploiting the obtained results in practical architectures for quantum information processing and quantum security. The achievement of these objectives will advance our understanding of quantum chaos from a

conceptual level to a practical and engineering one.

Acknowledgments

We gratefully acknowledge Mohsen Alishahiha and M.Javad Vasli for their discussions. The work of Reza Pirmoradian is based on research funded by the Iran National Science Foundation (INSF) under Project No. 4026389. Lastly, we recognize the use of AI tools in assisting with text editing and refinement.

References

- [1] L. Onsager, “Crystal Statistics. I. A Two-Dimensional Model with an Order-Disorder Transition,” *Phys. Rev.* **65**, no. 3–4, 117–149 (1944) doi:10.1103/PhysRev.65.117
- [2] E. Ising, “Contribution to the Theory of Ferromagnetism,” *Z. Phys.* **31**, 253–258 (1925) doi:10.1007/BF02980577
- [3] P. Jordan and E. P. Wigner, “About the Pauli exclusion principle,” *Z. Phys.* **47**, 631–651 (1928) doi:10.1007/BF01331938
- [4] H. Bethe, “On the theory of metals. 1. Eigenvalues and eigenfunctions for the linear atomic chain,” *Z. Phys.* **71**, 205–226 (1931) doi:10.1007/BF01341708
- [5] P. Pfeuty, “The one-dimensional Ising model with a transverse field,” *Annals Phys.* **57**, no.1, 79–90 (1970) doi:10.1016/0003-4916(70)90270-8
- [6] A. Polkovnikov, K. Sengupta, A. Silva and M. Vengalattore, “Colloquium: Nonequilibrium dynamics of closed interacting quantum systems,” *Rev. Mod. Phys.* **83**, no. 3, 863–883 (2011) doi:10.1103/RevModPhys.83.863
- [7] J. Eisert, M. Friesdorf and C. Gogolin, “Quantum many-body systems out of equilibrium,” *Nature Phys.* **11**, 124 (2015) doi:10.1038/nphys3215 [arXiv:1408.5148 [quant-ph]].
- [8] P. Calabrese and J. L. Cardy, “Time-dependence of correlation functions following a quantum quench,” *Phys. Rev. Lett.* **96**, 136801 (2006) doi:10.1103/PhysRevLett.96.136801 [arXiv:cond-mat/0601225 [cond-mat.stat-mech]].
- [9] P. Calabrese and J. Cardy, “Quantum Quenches in Extended Systems,” *J. Stat. Mech.* **0706**, P06008 (2007) doi:10.1088/1742-5468/2007/06/P06008 [arXiv:0704.1880 [cond-mat.stat-mech]].
- [10] M. Rigol, V. Dunjko and M. Olshanii, “Thermalization and its mechanism for generic isolated quantum systems,” *Nature* **452**, no. 7189, 854–858 (2008) doi:10.1038/nature06838 [arXiv:0708.1324 [cond-mat.stat-mech]].
- [11] M. Rigol, “Breakdown of Thermalization in Finite One-Dimensional Systems,” *Phys. Rev. Lett.* **103**, no. 10, 100403 (2009) doi:10.1103/PhysRevLett.103.100403 [arXiv:0904.3746 [cond-mat.stat-mech]].
- [12] J. M. Deutsch, “Quantum statistical mechanics in a closed system,” *Phys. Rev. A* **43**, no. 4, 2046–2049 (1991) doi:10.1103/PhysRevA.43.2046
- [13] R. Pirmoradian and M. R. Tanhayi, “Symmetry-resolved entanglement entropy for local and non-local QFTs,” *Eur. Phys. J. C* **84**, no.8, 849 (2024) doi:10.1140/epjc/s10052-024-13212-8 [arXiv:2311.00494 [hep-th]].

- [14] M. Srednicki, “Chaos and Quantum Thermalization,” *Phys. Rev. E* **50**, 888
doi:10.1103/PhysRevE.50.888 [arXiv:cond-mat/9403051 [cond-mat]].
- [15] H. Tasaki, “From Quantum Dynamics to the Canonical Distribution: General Picture and a Rigorous Example,” *Phys. Rev. Lett.* **80**, no. 7, 1373–1376 (1998)
doi:10.1103/PhysRevLett.80.1373
- [16] S. Goldstein, J. L. Lebowitz, R. Tumulka and N. Zanghi, “Canonical Typicality,” *Phys. Rev. Lett.* **96**, 050403 (2006) doi:10.1103/PhysRevLett.96.050403 [arXiv:cond-mat/0511091 [cond-mat.stat-mech]].
- [17] D. A. Huse, R. Nandkishore and V. Oganesyan, “Phenomenology of fully many-body-localized systems,” *Phys. Rev. B* **90**, no.17, 174202 (2014)
doi:10.1103/PhysRevB.90.174202 [arXiv:1408.4297 [cond-mat.stat-mech]].
- [18] R. Nandkishore and D. A. Huse, “Many body localization and thermalization in quantum statistical mechanics,” *Ann. Rev. Condensed Matter Phys.* **6**, 15-38 (2015)
doi:10.1146/annurev-conmatphys-031214-014726 [arXiv:1404.0686 [cond-mat.stat-mech]].
- [19] E. H. Lieb and D. W. Robinson, “The finite group velocity of quantum spin systems,” *Commun. Math. Phys.* **28**, 251-257 (1972) doi:10.1007/BF01645779
- [20] B. Nachtergaele and R. Sims, “Lieb-Robinson Bounds and the Exponential Clustering Theorem,” *Commun. Math. Phys.* **265**, no. 1, 119–130 (2006) doi:10.1007/s00220-006-1556-1 [arXiv:math-ph/0506030].
- [21] M. B. Hastings and T. Koma, “Spectral gap and exponential decay of correlations,” *Commun. Math. Phys.* **265**, 781-804 (2006) doi:10.1007/s00220-006-0030-4 [arXiv:math-ph/0507008 [math-ph]].
- [22] R. Barankov and A. Polkovnikov, “Microscopic diagonal entropy and its connection to basic thermodynamic relations,” *Annals Phys.* **326**, 486-499 (2011) doi:10.1016/j.aop.2010.08.004 [arXiv:0806.2862 [cond-mat.stat-mech]].
- [23] D. A. Abanin and Z. Papić, “Recent progress in many-body localization,” *Ann. Phys.* **529**, no. 7, 1700169 (2017) doi:10.1002/andp.201700169 [arXiv:1705.09103 [cond-mat.dis-nn]].
- [24] M. Alishahiha and M. J. Vasli, “Thermalization in Krylov basis,” *Eur. Phys. J. C* **85**, no.1, 39 (2025) doi:10.1140/epjc/s10052-025-13757-2 [arXiv:2403.06655 [quant-ph]].
- [25] L. D’Alessio, Y. Kafri, A. Polkovnikov and M. Rigol, “From quantum chaos and eigenstate thermalization to statistical mechanics and thermodynamics,” *Adv. Phys.* **65**, no.3, 239-362 (2016) doi:10.1080/00018732.2016.1198134 [arXiv:1509.06411 [cond-mat.stat-mech]].
- [26] C. H. Bennett, H. J. Bernstein, S. Popescu and B. Schumacher, “Concentrating partial entanglement by local operations,” *Phys. Rev. A* **53**, 2046-2052 (1996)
doi:10.1103/PhysRevA.53.2046 [arXiv:quant-ph/9511030 [quant-ph]].
- [27] D. N. Page, “Average entropy of a subsystem,” *Phys. Rev. Lett.* **71**, 1291-1294 (1993)
doi:10.1103/PhysRevLett.71.1291 [arXiv:gr-qc/9305007 [gr-qc]].
- [28] I. Affleck, “Universal Term in the Free Energy at a Critical Point and the Conformal Anomaly,” *Phys. Rev. Lett.* **56**, 746-748 (1986) doi:10.1103/PhysRevLett.56.746
- [29] R. Pirmoradian and M. R. Tanhayi, “Non-local probes of entanglement in the scale-invariant gravity,” *Int. J. Geom. Meth. Mod. Phys.* **18**, no.12, 2150197 (2021)
doi:10.1142/S0219887821501978 [arXiv:2103.02998 [hep-th]].

- [30] S. H. Shenker and D. Stanford, “Black holes and the butterfly effect,” *JHEP* **03**, 067 (2014) doi:10.1007/JHEP03(2014)067 [arXiv:1306.0622 [hep-th]].
- [31] J. Maldacena, S. H. Shenker and D. Stanford, “A bound on chaos,” *JHEP* **08**, 106 (2016) doi:10.1007/JHEP08(2016)106 [arXiv:1503.01409 [hep-th]].
- [32] P. Hayden and J. Preskill, “Black holes as mirrors: Quantum information in random subsystems,” *JHEP* **09**, 120 (2007) doi:10.1088/1126-6708/2007/09/120 [arXiv:0708.4025 [hep-th]].
- [33] A. Altland and M. R. Zirnbauer, “Nonstandard symmetry classes in mesoscopic normal-superconducting hybrid structures,” *Phys. Rev. B* **55**, no. 2, 1142–1161 (1997) doi:10.1103/PhysRevB.55.1142
- [34] J. J. M. Verbaarschot and T. Wettig, “Random matrix theory and chiral symmetry in QCD,” *Ann. Rev. Nucl. Part. Sci.* **50**, 343-410 (2000) doi:10.1146/annurev.nucl.50.1.343 [arXiv:hep-ph/0003017 [hep-ph]].
- [35] G. Vidal, “Efficient simulation of one-dimensional quantum many-body systems,” *Phys. Rev. Lett.* **93**, 040502 (2004) doi:10.1103/PhysRevLett.93.040502 [arXiv:quant-ph/0310089 [quant-ph]].
- [36] U. Schollwöck, “The density-matrix renormalization group in the age of matrix product states,” *Ann. Phys.* **326**, no. 1, 96–192 (2011) doi:10.1016/j.aop.2010.09.012 [arXiv:1008.3477 [cond-mat.str-el]].
- [37] R. Blatt and C. F. Roos, “Quantum simulations with trapped ions,” *Nature Phys.* **8**, 277-284 (2012) doi:10.1038/nphys2252
- [38] I. Bloch, J. Dalibard and S. Nascimbène, “Quantum simulations with ultracold quantum gases,” *Nature Phys.* **8**, 267-276 (2012) doi:10.1038/nphys2259
- [39] J. I. Cirac and P. Zoller, “Goals and opportunities in quantum simulation,” *Nat. Phys.* **8**, no. 4, 264–266 (2012) doi:10.1038/nphys2275
- [40] F. H. L. Essler and R. M. Konik, “Applications of massive integrable quantum field theories to problems in condensed matter physics,” doi:10.1142/9789812775344_0020 [arXiv:cond-mat/0412421 [cond-mat.str-el]].
- [41] C. Gogolin and J. Eisert, “Equilibration, thermalisation, and the emergence of statistical mechanics in closed quantum systems,” *Rept. Prog. Phys.* **79**, no.5, 056001 (2016) doi:10.1088/0034-4885/79/5/056001 [arXiv:1503.07538 [quant-ph]].
- [42] S. Sachdev and J. Ye, “Gapless spin-fluid ground state in a random quantum Heisenberg magnet,” *Phys. Rev. Lett.* **70**, no. 21, 3339–3342 (1993) doi:10.1103/PhysRevLett.70.3339 [arXiv:cond-mat/9212030].
- [43] P. Jurcevic, B. P. Lanyon, P. Hauke, C. Hempel, P. Zoller, R. Blatt and C. F. Roos, “Quasiparticle engineering and entanglement propagation in a quantum many-body system,” *Nature* **511**, no. 7508, 202–205 (2014) doi:10.1038/nature13461
- [44] J. K. Pachos and M. B. Plenio, “Three-Spin Interactions in Optical Lattices and Criticality in Cluster Hamiltonians,” *Phys. Rev. Lett.* **93**, no.5, 056402 (2004) doi:10.1103/PhysRevLett.93.056402 [arXiv:quant-ph/0401106 [quant-ph]].
- [45] M. Ghasemi, A. Naseh and R. Pirmoradian, “Odd entanglement entropy and logarithmic negativity for thermofield double states,” *JHEP* **10**, 128 (2021) doi:10.1007/JHEP10(2021)128 [arXiv:2106.15451 [hep-th]].

- [46] V. Eisler and I. Peschel, “Evolution of entanglement after a local quench,” *J. Stat. Mech.: Theory Exp.* **2007**, no. 06, P06005 (2007) doi:10.1088/1742-5468/2007/06/P06005 [arXiv:cond-mat/0703379 [cond-mat.stat-mech]].
- [47] H. Kim and D. A. Huse, “Ballistic Spreading of Entanglement in a Diffusive Nonintegrable System,” *Phys. Rev. Lett.* **111**, no.12, 127205 (2013) doi:10.1103/PhysRevLett.111.127205 [arXiv:1306.4306 [quant-ph]].
- [48] M. B. Hastings, “An area law for one-dimensional quantum systems,” *J. Stat. Mech.* **0708**, P08024 (2007) doi:10.1088/1742-5468/2007/08/P08024 [arXiv:0705.2024 [quant-ph]].
- [49] J. Cardy, “Quantum Quenches to a Critical Point in One Dimension: some further results,” *J. Stat. Mech.* **1602**, no.2, 023103 (2016) doi:10.1088/1742-5468/2016/02/023103 [arXiv:1507.07266 [cond-mat.stat-mech]].
- [50] P. Reimann, “Foundation of Statistical Mechanics under Experimentally Realistic Conditions,” *Phys. Rev. Lett.* **101**, no. 19, 190403 (2008) doi:10.1103/PhysRevLett.101.190403 [arXiv:0810.3092 [cond-mat.stat-mech]].
- [51] M. Rigol and L. Vidmar, “Generalized Gibbs ensemble in integrable lattice models,” *J. Phys. A* **2016**, no.6, 064007 (2016) doi:10.1088/1742-5468/2016/06/064007 [arXiv:1604.03990 [cond-mat.stat-mech]].
- [52] E. Ilievski, J. De Nardis, B. Wouters, J. S. Caux, F. H. L. Essler and T. Prosen, “Complete Generalized Gibbs Ensembles in an Interacting Theory,” *Phys. Rev. Lett.* **115**, no.15, 157201 (2015) doi:10.1103/PhysRevLett.115.157201 [arXiv:1507.02993 [quant-ph]].
- [53] B. Bertini, M. Collura, J. De Nardis and M. Fagotti, “Transport in Out-of-Equilibrium XXZ Chains: Exact Profiles of Charges and Currents,” *Phys. Rev. Lett.* **117**, no.20, 207201 (2016) doi:10.1103/PhysRevLett.117.207201 [arXiv:1605.09790 [cond-mat.stat-mech]].
- [54] R. Pirmoradian, E. Sadoogh, M. Teymouri, N. Abolqasemi-Azad, M. R. Lahooti and Z. Mohammad-Ali, “Investigation of quantum chaos in local and non-local Ising models,” [arXiv:2512.21713 [quant-ph]].
- [55] B. Swingle, G. Bentsen, M. Schleier-Smith and P. Hayden, “Measuring the scrambling of quantum information,” *Phys. Rev. A* **94**, no.4, 040302 (2016) doi:10.1103/PhysRevA.94.040302 [arXiv:1602.06271 [quant-ph]].
- [56] N. Y. Yao, F. Grusdt, B. Swingle, M. D. Lukin, D. M. Stamper-Kurn, J. E. Moore and E. A. Demler, “Interferometric Approach to Probing Fast Scrambling,” [arXiv:1607.01801 [quant-ph]].
- [57] F. Khorasani, R. Pirmoradian and M. R. Tanhayi, “Position dependence of Nielsen complexity for the thermofield double state,” *Phys. Lett. B* **851**, 138585 (2024) doi:10.1016/j.physletb.2024.138585 [arXiv:2308.15836 [quant-ph]].
- [58] I. García-Mata, R. A. Jalabert and D. A. Wisniacki, “Out-of-time-order correlators and quantum chaos,” *Scholarpedia* **18**, 55237 (2023) doi:10.4249/scholarpedia.55237 [arXiv:2209.07965 [quant-ph]].
- [59] A. J. Daley, H. Pichler, J. Schachenmayer and P. Zoller, “Measuring Entanglement Growth in Quench Dynamics of Bosons in an Optical Lattice,” *Phys. Rev. Lett.* **109**, no.2, 020505 (2012) doi:10.1103/PhysRevLett.109.020505 [arXiv:1205.1521 [cond-mat.quant-gas]].
- [60] D. A. Roberts and D. Stanford, “Diagnosing Chaos Using Four-Point Functions in

Two-Dimensional Conformal Field Theory,” *Phys. Rev. Lett.* **115**, no. 13, 131603 (2015) doi:10.1103/PhysRevLett.115.131603

- [61] B. Swingle and D. Chowdhury, “Slow scrambling in disordered quantum systems,” *Phys. Rev. B* **95**, no.6, 060201 (2017) doi:10.1103/PhysRevB.95.060201 [arXiv:1608.03280 [cond-mat.str-el]].
- [62] P. Hosur, X. L. Qi, D. A. Roberts and B. Yoshida, “Chaos in quantum channels,” *JHEP* **02**, 004 (2016) doi:10.1007/JHEP02(2016)004 [arXiv:1511.04021 [hep-th]].
- [63] R. Fan, P. Zhang, H. Shen and H. Zhai, “Out-of-time-order correlation for many-body localization,” *Science Bulletin* **62**, no. 10, 707–711 (2017) doi:10.1016/j.scib.2017.04.011 [arXiv:1608.01914 [cond-mat.quant-gas]].
- [64] M. Alishahiha, “On quantum complexity,” *Phys. Lett. B* **842**, 137979 (2023) doi:10.1016/j.physletb.2023.137979 [arXiv:2209.14689 [hep-th]].
- [65] D. A. Roberts and B. Yoshida, “Chaos and complexity by design,” *JHEP* **04**, 121 (2017) doi:10.1007/JHEP04(2017)121 [arXiv:1610.04903 [quant-ph]].
- [66] M. Doroudiani, A. Naseh and R. Pirmoradian, “Complexity for Charged Thermofield Double States,” *JHEP* **01**, 120 (2020) doi:10.1007/JHEP01(2020)120 [arXiv:1910.08806 [hep-th]].
- [67] R. Pirmoradian and M. R. Tanhayi, “On the Complexity of a Charged Quantum Oscillator,” *J. Korean Phys. Soc.* **77**, no. 2, 102–106 (2020). doi:10.3938/jkps.77.102 [arXiv:1911.08886 [physics.gen-ph]].
- [68] A. R. Brown and L. Susskind, “Second law of quantum complexity,” *Phys. Rev. D* **97**, no.8, 086015 (2018) doi:10.1103/PhysRevD.97.086015 [arXiv:1701.01107 [hep-th]].
- [69] M. J. Vasli, K. Babaei Velni, M. R. Mohammadi Mozaffar, A. Mollabashi and M. Alishahiha, “Krylov complexity in Lifshitz-type scalar field theories,” *Eur. Phys. J. C* **84**, no.3, 235 (2024) doi:10.1140/epjc/s10052-024-12609-9 [arXiv:2307.08307 [hep-th]].
- [70] A. Nahum, S. Vijay and J. Haah, “Operator Spreading in Random Unitary Circuits,” *Phys. Rev. X* **8**, no.2, 021014 (2018) doi:10.1103/PhysRevX.8.021014 [arXiv:1705.08975 [cond-mat.str-el]].
- [71] F. Khorasani, M. R. Tanhayi and R. Pirmoradian, “Ultimate limits to computation: anharmonic oscillator,” *Eur. Phys. J. Plus* **137**, no.6, 699 (2022) doi:10.1140/epjp/s13360-022-02900-7 [arXiv:2103.03124 [quant-ph]].
- [72] D. A. Roberts, D. Stanford and L. Susskind, “Localized shocks,” *JHEP* **03**, 051 (2015) doi:10.1007/JHEP03(2015)051 [arXiv:1409.8180 [hep-th]].
- [73] V. Khemani, D. A. Huse and A. Nahum, “Velocity-dependent Lyapunov exponents in many-body quantum, semiclassical, and classical chaos,” *Phys. Rev. B* **98**, no.14, 144304 (2018) doi:10.1103/PhysRevB.98.144304 [arXiv:1803.05902 [cond-mat.stat-mech]].
- [74] J. J. Garcia-Ripoll, “Time evolution of Matrix Product States,” [arXiv:cond-mat/0602305 [cond-mat.str-el]].
- [75] T. Rakovszky, F. Pollmann and C. W. von Keyserlingk, “Diffusive hydrodynamics of out-of-time-ordered correlators with charge conservation,” *Phys. Rev. X* **8**, no.3, 031058 (2018) doi:10.1103/PhysRevX.8.031058 [arXiv:1710.09827 [cond-mat.stat-mech]].
- [76] J. Cotler, N. Hunter-Jones, J. Liu and B. Yoshida, “Chaos, Complexity, and Random Matrices,” *JHEP* **11**, 048 (2017) doi:10.1007/JHEP11(2017)048 [arXiv:1706.05400 [hep-th]].

- [77] S. Paeckel, T. Köhler, A. Swoboda, S. R. Manmana, U. Schollwöck and C. Hubig, “Time-evolution methods for matrix-product states,” *Annals Phys.* **411**, 167998 (2019) doi:10.1016/j.aop.2019.167998 [arXiv:1901.05824 [cond-mat.str-el]].
- [78] V. Oganesyan and D. A. Huse, “Localization of interacting fermions at high temperature,” *Phys. Rev. B* **75**, no. 15, 155111 (2007) doi:10.1103/PhysRevB.75.155111 [arXiv:cond-mat/0610854 [cond-mat.str-el]].
- [79] F. Alet and N. Laflorencie, “Many-body localization: An introduction and selected topics,” *C. R. Physique* **19**, no. 6, 498–525 (2018) doi:10.1016/j.crhy.2018.03.003 [arXiv:1711.03145 [cond-mat.str-el]].
- [80] E. P. Wigner, “On the statistical distribution of the widths and spacings of nuclear resonance levels,” *Math. Proc. Cambridge Philos. Soc.* **47**, no. 4, 790–798 (1951) doi:10.1017/S0305004100027237
- [81] F. Haake, “Quantum Signatures of Chaos,” Springer, 2010, ISBN 978-3-642-26330-9, 978-3-642-05428-0 doi:10.1007/978-3-642-05428-0
- [82] J. M. Deutsch, “Eigenstate thermalization hypothesis,” *Rept. Prog. Phys.* **81**, no.8, 082001 (2018) doi:10.1088/1361-6633/aac9f1 [arXiv:1805.01616 [quant-ph]].
- [83] J. S. Cotler, G. Gur-Ari, M. Hanada, J. Polchinski, P. Saad, S. H. Shenker, D. Stanford, A. Streicher and M. Tezuka, “Black Holes and Random Matrices,” *JHEP* **05**, 118 (2017) [erratum: *JHEP* **09**, 002 (2018)] doi:10.1007/JHEP05(2017)118 [arXiv:1611.04650 [hep-th]].
- [84] D. J. Thouless, “Maximum Metallic Resistance in Thin Wires,” *Phys. Rev. Lett.* **39**, no. 18, 1167–1169 (1977) doi:10.1103/PhysRevLett.39.1167
- [85] T. Guhr, A. Muller-Groeling and H. A. Weidenmuller, “Random matrix theories in quantum physics: Common concepts,” *Phys. Rept.* **299**, 189-425 (1998) doi:10.1016/S0370-1573(97)00088-4 [arXiv:cond-mat/9707301 [cond-mat]].
- [86] W. Beugeling, R. Moessner and M. Haque, “Finite-size scaling of eigenstate thermalization,” *Phys. Rev. E* **89**, no.4, 042112 (2014) doi:10.1103/PhysRevE.89.042112 [arXiv:1308.2862 [cond-mat.stat-mech]].
- [87] J. R. Garrison and T. Grover, “Does a single eigenstate encode the full Hamiltonian?,” *Phys. Rev. X* **8**, 021026 (2018) doi:10.1103/PhysRevX.8.021026 [arXiv:1503.00729 [cond-mat.str-el]].
- [88] J. Martin, O. Giraud and B. Georgeot, “Multifractality and intermediate statistics in quantum maps,” *Phys. Rev. E* **77**, no. 3, 035201 (2008) doi:10.1103/PhysRevE.77.035201
- [89] R. Pirmoradian, M. H. Bek-Khoshnevis, S. Ebadi and M. R. Tanhayi, “Entanglement Structure of Nonlocal Field Theories,” [arXiv:2511.10505 [quant-ph]].
- [90] H. Li and F. D. M. Haldane, “Entanglement Spectrum as a Generalization of Entanglement Entropy: Identification of Topological Order in Non-Abelian Fractional Quantum Hall Effect States,” *Phys. Rev. Lett.* **101**, no. 1, 010504 (2008) doi:10.1103/PhysRevLett.101.010504 [arXiv:0805.0332 [cond-mat.mes-hall]].
- [91] I. Peschel, “Special Review: Entanglement in Solvable Many-Particle Models,” *Braz. J. Phys.* **42**, no.3, 267-291 (2012) doi:10.1007/s13538-012-0074-1 [arXiv:1109.0159 [cond-mat.stat-mech]].
- [92] S. H. Shenker and D. Stanford, “Stringy effects in scrambling,” *JHEP* **05**, 132 (2015) doi:10.1007/JHEP05(2015)132 [arXiv:1412.6087 [hep-th]].

- [93] R. Islam, R. Ma, P. M. Preiss, M. E. Tai, A. Lukin, M. Rispoli and M. Greiner, “Measuring entanglement entropy through the interference of quantum many-body twins,” doi:10.1038/nature15750 [arXiv:1509.01160 [cond-mat.quant-gas]].
- [94] H. Bernien, S. Schwartz, A. Keesling, H. Levine, A. Omran, H. Pichler, S. Choi, A. S. Zibrov, M. Endres and M. Greiner, *et al.* “Probing many-body dynamics on a 51-atom quantum simulator,” Nature **551**, 579-584 (2017) doi:10.1038/nature24622 [arXiv:1707.04344 [quant-ph]].
- [95] J. Smith, A. Lee, P. Richerme, B. Neyenhuis, P. W. Hess, P. Hauke, M. Heyl, D. A. Huse and C. Monroe, “Many-body localization in a quantum simulator with programmable random disorder,” Nature Phys. **12**, no.10, 907-911 (2016) doi:10.1038/nphys3783 [arXiv:1508.07026 [quant-ph]].